

# Improving nitrogen cycling in a land surface model (CLM5) to quantify soil N<sub>2</sub>O, NO and NH<sub>3</sub> emissions from enhanced rock weathering with croplands

Maria Val Martin<sup>1</sup>, Elena Blanc-Betes<sup>2,3</sup>, Ka Ming Fung<sup>4</sup>, Euripides P. Kantzas<sup>1</sup>, Ilsa B. Kantola<sup>2,3</sup>,  
5 Isabella Chiaravalloti<sup>5</sup>, Lyla T. Taylor<sup>1</sup>, Louisa K. Emmons<sup>6</sup>, William R. Wieder<sup>6,7</sup>, Noah J. Planavsky<sup>5</sup>,  
Michael D. Masters<sup>2,3</sup>, Evan H. DeLucia<sup>2,3,8</sup>, Amos P.K. Tai<sup>4,9</sup> and David J. Beerling<sup>1</sup>

<sup>1</sup>Leverhulme Centre for Climate Change Mitigation, School of Biosciences, University of Sheffield, Sheffield, UK

<sup>2</sup>Institute for Sustainability, Energy, and Environment, University of Illinois at Urbana-Champaign, Urbana, IL, USA

<sup>3</sup>Carl R. Woese Institute for Genomic Biology, University of Illinois at Urbana-Champaign, Urbana, IL, USA

10 <sup>4</sup>Earth and Environmental Sciences Programme, Faculty of Science, The Chinese University of Hong Kong, Sha Tin, Hong Kong

<sup>5</sup>Department of Earth and Planetary Sciences, Yale University, New Haven, CT, USA

<sup>6</sup>National Center for Atmospheric Research, Boulder, CO, USA

<sup>7</sup>Institute of Arctic and Alpine Research, University of Colorado Boulder, Boulder CO, USA

15 <sup>8</sup>Department of Plant Biology, University of Illinois at Urbana-Champaign, Urbana, IL, USA

<sup>9</sup>State Key Laboratory of Agrobiotechnology and Institute of Environment, Energy and Sustainability, The Chinese University of Hong Kong, Sha Tin, Hong Kong

*Correspondence to:* Maria Val Martin (m.valmartin@sheffield.ac.uk)

20 **Abstract.** Surficial enhanced rock weathering (ERW) is a land-based carbon dioxide removal (CDR) strategy that involves applying crushed silicate rock (e.g., basalt) to agricultural soils. However, unintended biogeochemical interactions with the nitrogen cycle may arise through ERW increasing soil pH as basalt grains undergo dissolution that may reinforce, counteract, or even offset the climate benefits from carbon sequestration. Increases in soil pH could drive changes in the soil emissions of key non-CO<sub>2</sub> greenhouse gases, e.g., nitrous oxide (N<sub>2</sub>O), and trace gases, e.g., nitric oxide (NO) and ammonia (NH<sub>3</sub>) that  
25 affect air quality, and crop and human health. We present the development and implementation of a new improved nitrogen cycling scheme for the land surface model Community Land Model v5 (CLM5), the land component of the Community Earth System Model, allowing evaluation of ERW effects on soil gas emissions. We base the new parameterizations on datasets derived from soil pH responses of N<sub>2</sub>O, NO and NH<sub>3</sub> of ERW field trial and mesocosm experiments with crushed basalt. We successfully validated simulated ‘control’ (i.e., no ERW) seasonal cycles of soil N<sub>2</sub>O, NO and NH<sub>3</sub> emissions against a wide  
30 range of global emission inventories. We benchmark simulated mitigation of soil N<sub>2</sub>O fluxes in response to ERW against a sub-set of data from ERW field trials in the U.S. Corn Belt. Using the new scheme, we provide a specific example of the effect of large-scale ERW deployment with croplands on soil nitrogen fluxes across five key regions with high potential for CDR with ERW (North America, Brazil, Europe, India, and China). Across these regions, ERW implementation led to marked reductions in N<sub>2</sub>O and NO (both 18%) with moderate increases in NH<sub>3</sub> (2%). Our improved N-cycle scheme within CLM5 has  
35 utility for investigating the potential of ERW point-source and regional effects of soil N<sub>2</sub>O, NO and NH<sub>3</sub> fluxes in response to

current and future climates. This framework also provides the basis for assessing the implications of ERW for air quality given the role of NO in tropospheric ozone formation, and both NO and NH<sub>3</sub> in inorganic aerosol formation.

## 1 Introduction

40 Drastic and rapid emission reductions and the use of carbon dioxide (CO<sub>2</sub>) removal (CDR) technologies are essential for meeting the Paris Agreement on Climate and net-zero commitments (IPCC, 2021). Modelled scenarios indicate that 7-15 gigatons (Gt) of CO<sub>2</sub> must be removed and safely stored each year to limit warming to 2°C (Riahi et al, 2021). A series of land-based CDR strategies involving the terrestrial biosphere have been proposed, which includes afforestation and reforestation, bioenergy crops, enhanced rock weathering (ERW) and peatland restoration, among others. An overview of these land-based CDR strategies and recommendations for their application have been summarized by independent international expert committees (e.g., National Research Council, 2015, Royal Society, 2018, Smith et al., 2023) as well as the IPCC 2021 45 report (Canadell et al., 2021). All these reports agree that there are unidentified environmental risks that must be assessed, because they may reinforce, counteract, or even offset the climate benefits from carbon sequestration.

Land-based enhanced rock weathering is a CDR strategy, which involves applying crushed silicate rock (e.g., basalt) to soils to sequester carbon, and is potentially feasible for large-scale deployment with managed croplands and grazing lands. Basalt 50 is an ideal abundant silicate rock for ERW because of its potential co-benefits for crop yields and capacity to reverse soil acidification (Kantola et al., 2017; Beerling et al., 2018) and supply plant-essential nutrients like phosphorus (Goll et al., 2021). The estimated global net CDR potential for ERW deployed on main crop regions worldwide is 0.5–2 Gt CO<sub>2</sub> yr<sup>-1</sup> with extraction costs of US\$80–180 per tonne of CO<sub>2</sub> and carbon storage time scales of ≥10,000 years (Beerling et al., 2020). However, interactions between ERW, nitrogen (N) cycling, and soil-plant processes lead to changes in the emissions of other 55 greenhouse gases (GHGs), e.g., nitrous oxide (N<sub>2</sub>O), methane (CH<sub>4</sub>), and atmospheric pollutants, e.g., nitrogen oxides (NO<sub>x</sub>=NO+NO<sub>2</sub>) and ammonia (NH<sub>3</sub>) from soils.

N<sub>2</sub>O is an important greenhouse gas and a long-lived stratospheric ozone-depleting substance (Prather et al., 2015). The concentration of atmospheric N<sub>2</sub>O has increased by more than 20% during the last centuries and is currently increasing at a rate of 2% per decade (Tian et al., 2020). Agricultural ecosystems are the largest anthropogenic source of N<sub>2</sub>O, with about 60 50% of the global emissions (Tian et al., 2020). Agricultural ecosystems are also significant sources of NH<sub>3</sub> and NO<sub>x</sub>, comprising about 80% of global NH<sub>3</sub> emissions (Van Damme et al., 2021) and about 10% of global NO<sub>x</sub> emissions (IPCC, 2021). Once emitted from soil, NH<sub>3</sub> and NO<sub>x</sub> species can lead to air pollution, by increasing N deposition as well as production of other air pollutants, such as ozone (O<sub>3</sub>) and particulate matter (PM, as PM<sub>2.5</sub> with particles with an aerodynamic diameter <2.5 μm and PM<sub>10</sub> with diameter <10 μm), which are harmful to human, ecosystem, and crop health. These nitrogen trace 65 gases can also contribute to water eutrophication, soil acidification and loss of plant species and habitat diversity (e.g., Sutton et al., 2009). In the coming decades, soil nitrogen emissions in croplands are expected to continue to increase because of

fertilizer and manure application to meet the growing demand for food, forage, fibre, and energy (e.g., Reay et al., 2012; Davidson and Kanter, 2014; IPCC, 2021).

70 In agriculture ecosystems, soil  $\text{N}_2\text{O}$  and  $\text{NO}$  fluxes are driven by two main biochemical processes: nitrification and denitrification, while soil  $\text{NH}_3$  is driven by volatilization. These three processes are controlled by many environmental factors such as temperature, soil pH, water and oxygen content and N availability (via synthetic fertilizer and manure applications) (e.g., Reay et al., 2012; Tian et al., 2016). Analyses from enhanced weathering field experiments in the U.S. Corn Belt have shown that the application of basalt consistently increases soil pH and reduces soil  $\text{N}_2\text{O}$  fluxes with no effects on soil  $\text{CO}_2$  emissions (Blanc-Betes et al., 2020). It is expected that increases in soil pH will concurrently produce a decrease in soil  $\text{NO}_x$  emissions, by decreasing rates of denitrification and nitrification (Parson et al., 2001) and an increase in  $\text{NH}_3$  volatilization (Mkhabela et al., 2006). Thus, widespread implementation of ERW holds consequences for air quality and human and crop health as well as for climate mitigation that have so far been overlooked. To date, there is no modelling framework that has the capability to fully quantify the changes in biogeochemical processes and atmospheric trace gas emissions from ERW applications.

80 In this study, we present the development and implementation of a new improved N cycling scheme for the land surface model Community Land Model v5 (CLM5), the land component of the Community Earth System Model, allowing evaluation of ERW effects on soil nitrogen gas emissions. We base the new parameterizations on datasets derived from soil pH responses of  $\text{N}_2\text{O}$ ,  $\text{NO}$  and  $\text{NH}_3$  in ERW field trial and mesocosm experiments with crushed basalt. Finally, we present a case examining the impact of large-scale deployment of ERW on main croplands across the world on  $\text{N}_2\text{O}$ ,  $\text{NO}$  and  $\text{NH}_3$  emissions.

## 85 **2 Methodology**

### **2.1 The Community Land Model version 5 (CLM5)**

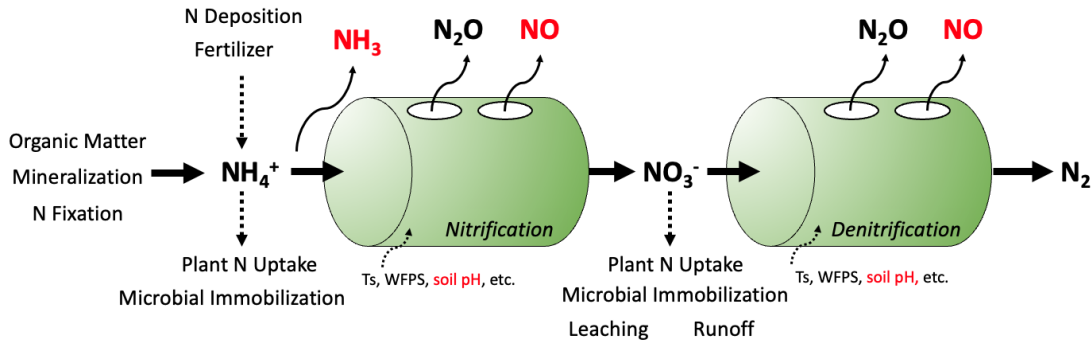
We implemented new parameterizations into the Community Land Model version 5.0.25 (CLM5; Lawrence et al., 2019) to determine  $\text{N}_2\text{O}$  and  $\text{NO}$  fluxes, and  $\text{NH}_3$  volatilized from soil due to basalt amendments in crops. CLM is the terrestrial component of the Community Earth System Model version 2 (CESM2; Danabasoglu et al., 2020). CLM5 represents terrestrial carbon and nitrogen cycling with prognostic vegetation and crop growth. The model uses a sub-grid hierarchy in which grid cells are composed of multiple land units, columns, and patches to represent the spatial land surface heterogeneity and the biogeophysical and biogeochemical differences between various land types within a model grid cell. The CLM5 land units are vegetated, lake, urban, glacier, and crop. Vegetation and crops are represented by plant and crop functional types (PFTs and CFTs), each with its own set of ecophysiological, morphological, phenological, and biogeochemical parameters (Levis et al., 95 2018). The default PFT distribution of natural vegetation and crops are derived from satellite observations (e.g., MODIS) and agricultural census data (Lawrence and Chase, 2007; Portmann et al., 2010). There are 16 types of natural vegetation (including bare ground) and eight active crops (temperate soybean, tropical soybean, temperate corn, tropical corn, spring wheat, cotton,

rice, and sugarcane) (Lombardozi et al., 2020). In CLM5, natural vegetation and croplands are treated on separate columns and isolate particular management practices, i.e., natural vegetation is handled in single unmanaged soil columns sharing a  
100 single pool of water and nutrients, whereas each crop has a dedicated column (Drewniak et al., 2013).

For crops, CLM5 provides nutrients from the mineral N pool in the soil, which is supplied through organic matter decomposition, N deposition, N fixation and fertilization. The interactive N fertilization scheme in CLM5 simulates fertilization by adding N directly to the soil mineral  $\text{NH}_4^+$  pool to meet crop N demands using both synthetic fertilizer and manure application. Fertilizer is applied to each crop for 20 successive days uniformly as soon as the crops enter the leaf  
105 emergence phase and is added in each layer from ground surface to 0.4 m depth according to the model-defined soil profile (Lawrence et al., 2019). CLM5 simulates the beginning of plant growth stages (seedling, leaf emerging, and grain filling) as well as crop sowing dates and planting durations based on the cumulative warm-enough hours at the beginning of spring. Crops are harvested once they reach maturity or a predefined maximum growing days (typically 150–165 days) (Lawrence et al., 2019; Lombardozi et al., 2020).

## 110 **2.2 Updates and implementations in the soil nitrogen scheme**

Figure 1 summarizes the main processes of the terrestrial N cycle in CLM5, following the ‘holes-in-a-pipe’ concept (e.g., Firestone and Davidson, 1989; Davidson and Verchot, 2000; Inatomi et al., 2019), highlighting the main implementations in this work. The model tracks N content in soil, plants, and organic matter as a series of distinct N pools, with biogeochemical processes acting as N exchange fluxes across them. Soil N transformations occur in vertically resolved soil profiles in each  
115 soil column following a Century-like implementation of soil biogeochemistry (Koven et al., 2013; Lawrence et al., 2019). Plant uptake, microbial immobilization, N mineralization, nitrification, and denitrification compete for soil mineral nitrogen ( $\text{NH}_4^+$  and  $\text{NO}_3^-$ ) based on the relative demand from each process. The release of  $\text{N}_2\text{O}$  as byproduct of nitrification and denitrification, and the leaching of soil nitrate ( $\text{NO}_3^-$ ) result in N losses from terrestrial ecosystems, which are replaced through fertilization, atmospheric N deposition, and biological N fixation (both symbiotic and asymbiotic). In this study, we modify  
120 CLM5 to better simulate the terrestrial nitrogen cycle by implementing soil  $\text{NO}$  fluxes and  $\text{NH}_3$  from volatilization and integrating regulating functions of soil pH that allows to evaluate the potential impact of basalt amendments on soil nitrogen gas fluxes.



125 **Figure 1: Conceptual diagram of nitrogen cycle and the “holes-in-a-pipe” approach. Parameters in red are new additions in the default model. Ts is soil temperature; WFPS is water-filled pore space; and N is nitrogen.**

### 2.2.1 Inorganic N transformations, soil N<sub>2</sub>O fluxes and soil pH

Nitrification and denitrification processes in CLM5 are based on the process-based biogeochemical model DAYCENT (Parton et al., 1996; Del Grosso et al., 2000; Del Grosso et al., 2006). For nitrification fluxes, we included the dependency of N mineralization-based term on potential nitrification rates that was implemented in Parton et al. (2001), which was missing from  
 130 previous versions of CLM5 (Nevison et al., 2022a). Under this scheme, 20% of mineralized nitrogen is nitrified.

CLM5 assumes a constant fraction to be N<sub>2</sub>O produced from nitrification ( $fN_{2O_{nit}} = 6 \times 10^{-4}$ ; Li et al., 2000). However, this N<sub>2</sub>O production depends on environmental conditions like soil temperature, water content and pH (Inatomi et al., 2020 and references therein). Considering an independent N<sub>2</sub>O emission fraction linked to environmental conditions provide better estimates of N<sub>2</sub>O emissions. To incorporate the effect of basalt addition on nitrification N<sub>2</sub>O fluxes via regulating soil pH, we  
 135 adopted a modified pH-based function ( $fN_{2O_{nit}}$ ) proposed by Inatomi et al., (2020) based on a meta-analysis:

$$fN_{2O_{nit}} = 721.86 \times e^{-2.387 \times \text{pH}}$$

The updated  $fN_{2O_{nit}}$  function made the nitrification rate in CLM5 go from the global constant average of 0.06% to 0.3% and increased the global N<sub>2</sub>O nitrification/denitrification ratio from 1% to 14%, more accordingly to previous estimates (Inatomi et al., 2020). It should be noted that  $fN_{2O_{nit}}$  values at typical soil pH levels in croplands (5.8 to 6.2) fall within a relatively  
 140 narrow range of  $3$  to  $7 \times 10^{-4}$ , which is not significantly different from the original  $6 \times 10^{-4}$  implemented in the model. Small variations in  $fN_{2O_{nit}}$  (e.g.,  $\pm 20\%$ ) have a negligible impact on the total soil N<sub>2</sub>O fluxes, with changes ranging 0.04 to 0.3%. However, further work is needed to evaluate the sensitivity of the model to this specific parameterization under other soil conditions, as well as to incorporate the influence of other environmental factors, such as water content and temperature.

As CLM5 uses a fixed pH value of 6.5 across all soils (Lawrence et al., 2019), we implemented the global soil pH from the  
 145 Harmonized World Soil Database (FAO, 2012; Wieder et al., 2014). This dataset provides global spatial distribution of soil

pH and other soil properties for surface (0 to 30cm) and deeper soils (30 to 100 cm) at 0.05-degree spatial resolution, and regridded to the CLM5 resolution (0.9x1.25) for the nominal year of 2000 (Fig. S1 in Supplementary Material (SM)). We further distributed the topsoil and subsoil soil pH values through the CLM5 soil layers accordingly.

Denitrification also produces N<sub>2</sub>O as a byproduct (Fig. 1). To model the effect of basalt addition on N<sub>2</sub>O fluxes from denitrification, we included the updated denitrification scheme of Blanc-Betes et al., (2020). As in CLM5, Blanc-Betes et al., (2020)'s scheme is a modified version of the DAYCENT denitrification subroutine (Parton et al., 1996; Del Grosso et al., 2000) with the difference that it incorporates the effects of soil pH on gross denitrification rates (N<sub>2</sub> + N<sub>2</sub>O) and on the stoichiometry of denitrification end products (R<sub>N<sub>2</sub>:N<sub>2</sub>O</sub> ratio).

For the total N loss during denitrification, the pH effect function ( $f_{pH}$ ) was based on Liu et al. (2010) and Rochester (2003):

$$f_{pH} = 0.0016e^{1.006 \times \text{pH}}$$

For the N<sub>2</sub> to N<sub>2</sub>O ratio of the end products, we included the pH effect function ( $f_{pH}$ ) adapted from Wagena et al. (2017) with adjusted thresholds:

$$f_{pH} = \begin{cases} 0.001 & \text{for pH} \leq 4 \\ 0.001 + \frac{\text{pH} - 4}{3} & \text{for } 4 < \text{pH} < 7 \\ 1.0 & \text{for pH} \geq 7 \end{cases}$$

More information about the scheme, model calibration and validation with basalt observations in crops is provided by Blanc-Betes et al (2020).

### 2.2.2 Soil NO fluxes

In addition to the modifications in the N<sub>2</sub>O scheme, we implemented a new parameterization to calculate NO released as by-products of nitrification and denitrification. We used the ratio of NO to N<sub>2</sub>O to account for the emission of NO during nitrification and denitrification based on Parton et al., (2001) and Zhao et al., (2017):

$$R_{\text{NO:N}_2\text{O}} = 15.2 + \frac{35.5 \tan^{-1}[0.75\pi(10D_r - 1.86)]}{\pi},$$

where  $D_r$  is the soil relative gas diffusivity in soil with respect to air and is calculated as a function of air-filled pore space (AFPS) of soil (Davidson and Trumbore, 1995):

$$D_r = 0.209 \text{AFPS}^{\frac{4}{3}},$$

where AFPS is  $1 - \frac{\theta_v}{\theta_{v,\text{sat}}}$  and  $\theta_v$  and  $\theta_{v,\text{sat}}$  are instantaneous and saturated volumetric soil water content (in m<sup>3</sup> m<sup>-3</sup>), respectively.

NO emitted from soils is quickly oxidized to NO<sub>2</sub> by O<sub>3</sub> near the canopy, and the formed NO<sub>2</sub> may be deposited onto the plant canopy (Bakwin et al., 1990; Jacob and Wofsy, 1990). To account for the loss of NO to plant canopy, we applied a canopy reduction scaling factor (CRF; Fig. S2 in SM) based on Yan et al (2005):

$$\text{CRF} = \frac{e^{-K_S \times \text{SAI}} + e^{-K_C \times \text{LAI}}}{2},$$

175 where SAI and LAI are stomatal area index and leaf area index, respectively, and  $k_s$  and  $k_c$  are 11.6 and 0.32, respectively. The corresponding SAI was derived from the SAI:LAI ratio of Yienger and Levy (1995). NO captured from the atmosphere is taken up by the plant system either by direct incorporation into the leaf tissues or by the roots after absorption into the soil (Yoneyama et al., 1980). Since the precise mechanisms underlying these two routes is uncertain and fall outside the scope of this study, we assumed that all captured NO is returned to the soil directly as NH<sub>4</sub><sup>+</sup>.

180 We also included a rain pulse factor to the base NO flux associated with nitrification to simulate the rapid increase of NO fluxes following rain onto a previous dry soil period (e.g., Parton et al., 2001; Yan et al., 2005; Hudman et al., 2012) as:

$$P_{peak} = 13.01 \ln(l_{dry}) - 53.6 \times e^{-ct},$$

where  $P_{peak}$  represents the magnitude of the peak flux relative to the pre-wetting flux and the value of  $l_{dry}$  is the antecedent dry period in hours. The  $c$  is a rate constant representing the rise/fall time of the pulse (0.068 h<sup>-1</sup>) and  $t$  is time-step in hours.  $P_{peak}$  depends logarithmically on the length of the antecedent dry period and the condition for a pulse is a change in soil moisture. 185 To test for pulsing potential, we employed the two-part condition as in Yan et al., (2005). Dry soil is defined as soils with a moisture content below 17.5% (v/v). To trigger a pulse, an increase of more than 0.5% (v/v) in the moisture content of soil that experiences dry conditions for at least 3 days is required. This increase of 0.5% (v/v) in 7 cm of surface soil is equivalent to about 3.5 mm of rainfall, which is the rainfall amount previously reported to cause a pulse (e.g., Johansson and Sanhueza, 190 1988; Martin et al., 1998).

Following Parton et al., (2001), total NO emissions from soils and released above canopy are thus calculated as a function of the simulated N<sub>2</sub>O fluxes, the  $R_{\text{NO:N}_2\text{O}}$  function, the factor to account for rain pulses in NO emission initiated by precipitation events ( $P$ ) and the CRF:

$$\text{Soil NO}_{\text{soil}} = \text{N}_2\text{O}_{\text{denit}} \times R_{\text{NO:N}_2\text{O}} + \text{N}_2\text{O}_{\text{nit}} \times R_{\text{NO:N}_2\text{O}} \times P$$

$$195 \quad \text{Soil NO}_{\text{above-canopy}} = \text{Soil NO}_{\text{soil}} \times \text{CRF}$$

### 2.2.3 Soil NH<sub>3</sub> volatilization

For NH<sub>3</sub> volatilization, we used the scheme implemented by Fung et al., (2022) and embedded within the CLM5 N cycle. This scheme is derived from the DeNitrification-DeComposition (DNDC) biogeochemical model (Li et al., 2012) and includes a further parameterization to account for released NH<sub>3</sub> that is captured in the plant canopy. As in the soil NO scheme, we assumed

200 all captured  $\text{NH}_3$  returns to the soil directly as  $\text{NH}_4^+$ . In this scheme,  $\text{NH}_3$  is very sensitive to soil pH, as it grows exponentially with pH, in the order of  $10^{\text{pH}}$ . As shown by Fung et al., (2022), the use of a spatially distributed soil pH database is not feasible as it overestimates  $\text{NH}_3$  fluxes in alkaline soils ( $\text{pH} > 6.5$ ). This is a well-known limitation in current  $\text{NH}_3$  schemes (e.g., Sutton et al., 2013; Vira et al., 2020), where functions are not parameterized for global applications, and further work is needed for global models to accurately describe soil pH effects on  $\text{NH}_3$  fluxes. In this work, we kept the soil pH constant to 6.5 to estimate  
205 a consistent  $\text{NH}_3$  flux baseline and added a unit factor ( $f_{\text{pH}}$ ) as a function of soil pH to model the effect of basalt addition on  $\text{NH}_3$  fluxes. The new regulating  $f_{\text{pH}}$  function is based on previous observations of  $\text{NH}_3$  and soil pH from lime (Mkhabela et al., 2006), biochar (Kim et al., 2021) and basalt applications (Chiaravalloti, 2023) (Fig. S3 in SM):

$$f_{\text{pH}} = \begin{cases} 0.6 & \text{for pH} < 5 \\ 0.6 + \frac{0.4}{3} \times (\text{pH} - 5) & \text{for } 5 \geq \text{pH} \leq 8 \\ 1.0 & \text{for pH} > 8 \end{cases}$$

This function is a first approximation, which allows releasing some  $\text{NH}_3$  in very acidic crop soils ( $\text{pH} < 5.5$ ), whereas  
210 increasingly  $\text{NH}_3$  volatilization losses occur in higher soil pH with a saturation at relatively high soil pH levels ( $>8$ ). Observations on the magnitude of soil pH in controlling  $\text{NH}_3$  volatilization fluxes from basalt applications are very scarce. However, our proposed changes in  $f_{\text{pH}}$  are fairly consistent with soil pH effects in  $\text{NH}_3$  volatilization observed in field measurements in a marshland soil with lime application (Mkhabela et al., 2006), experimental measurements from basalt application ( $12.5 \text{ t rock ha}^{-1}$ ) in a greenhouse setting (Chiaravalloti, 2023) and chamber experiments with 3% biochar and  
215 liquid fertilizers (Kim et al., 2021). Further observations of  $\text{NH}_3$  volatilization rates from basalt application under wider range of soil pH conditions are urgently needed to verify the actual effect of soil pH.

### 2.3 CLM5 ERW simulations

We performed single-point simulations at the Energy Farm field site (University of Illinois, U.S.) to examine the model sensitivity to basalt applications in maize and soybean crops and soil and climate conditions. We spun-up the model for about  
220 600 years, so that all the state variables in the model, especially total ecosystem soil carbon and soil  $\text{N}_2\text{O}$  reached equilibrium. Then, the same initial condition was used for both the soybean and the corn single-point present-day spin-up simulations because a uniform soil condition was achieved for both crop systems. The present-day spin-up was based on a historical simulation 1850–2014, using historical N and aerosol deposition, atmospheric  $\text{CO}_2$  forcing and meteorological forcings from GSWP3 version (Lawrence et al., 2019), with soil texture and soil pH values based on onsite measurements in Control and  
225 ERW plots at the Energy Farm (Blanc-Betes et al., 2020). Following the historical simulation, the Energy Farm simulations were run from 2015 to 2019 with meteorological forcing data retrieved from the North American Land Data Assimilation System (NLDAS) forcing dataset (Xia et al., 2012), and initial conditions starting in 2015 for the two single-point simulations, without basalt ('Control' Run) and with basalt ('ERW' Run) application. The use of two different atmospheric forcings,



GSWP3 (1901-2014) and NLDAS (1999-2020), was necessary in this study due to their distinct time coverage. Although this  
230 approach has the potential to introduce biases and changes in soil dynamics, we conducted a comparison for a coincidental  
period (2001-2014) and found no significant impacts on vegetation, soil nitrogen fluxes and soil dynamics (Fig. S4 in SM).

In addition to single-point simulations, we performed global simulations to validate the new implementation at large scale and  
assess the regional effects of basalt treatments to soil direct agricultural N fluxes. We first spun-up CLM5 with the new  
implementations to steady state in 1850 using an accelerated decomposition procedure and fixed pre-industrial CO<sub>2</sub>, land use,  
235 and atmospheric N deposition (Lawrence et al., 2019). The accelerated decomposition spin-up was for about 1200 years and  
we considered the model fully spun-up when the land surface had more than 97% of the total ecosystem carbon in equilibrium.  
After the historical spin-up, we initialized CLM5 simulations for 2000 using fully spun-up conditions. The present-day spin-  
up was based on a historical simulation 1850–2014, using historical N and aerosol deposition, atmospheric CO<sub>2</sub> forcing, and  
240 version 1; <http://hydro.iis.u-tokyo.ac.jp/GSWP3/>), with forcing data available from 1901 to 2014 and cycled from 1901 to  
1920 for years prior to 1901.

To model the effect of basalt addition on the N<sub>2</sub>O, NO and NH<sub>3</sub> fluxes from soil, we developed a weathering option for CLM5,  
in which annual or monthly changes in soil pH estimated by an ERW model offline (Beerling et al., 2020; Kantzas et al., 2022)  
are read within the CLM5 N cycle. Specifically, CLM5 acquires spatially distributed delta pH values, and adjusts the initial  
245 soil pH accordingly. Thus, in the “Control” Run soil pH is kept constant to the nominal values provided by Harmonized World  
Soil Database, whereas in the “ERW” Run is modified following the ERW model projection. In this work, we considered the  
soil pH changes as well as application locations across five key regions with high potential for CDR with ERW (North America,  
Brazil, Europe, India, and China) required to remove 2Gt CO<sub>2</sub> per year (Beerling et al., 2020). To test the new scheme at a  
global scale, we used changes in annual soil pH (Fig. 2 and Fig. S5 in SM); dynamic changes of soil pH in monthly timesteps  
250 were tested in a regional study for the UK (Kantzas et al., 2022).

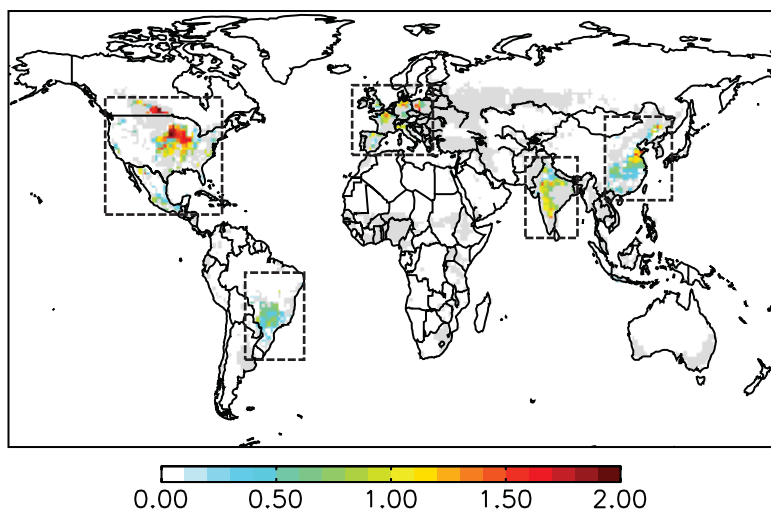


**Figure 2: Changes in soil pH after annual basalt applications in a 25-year timeframe to remove 2 Gt CO<sub>2</sub> (Beerling et al., 2020). Delimited are the five agriculture regions considered in this study; shaded in grey are grid cells with crops (> 10%), in which basalt was not applied. A close-up view for each region is in Figure S5 in SM.**

255 Simulations were completed at a resolution of 0.9° latitude by 1.25° longitude and with a 30-min time step. We used the mean and standard deviation of the last 5 years (2010–2014) of the historical simulations as an approximation of present-day conditions of the modelled N cycle, for a Control Run (without basalt) and an ERW Run (with basalt). In both simulations, synthetic fertilizer application was prescribed by crop type on the Land Use Model Intercomparison Project (Hurtt et al., 2011) and manure fertilizer was applied at a fixed rate for all crops (20 kg N ha<sup>-1</sup> yr<sup>-1</sup>; Lombardozzi et al., 2020).

## 260 **2.6 Datasets for model validation**

We used observational data collected at the University of Illinois Energy Farm in 2016–2019. The Energy Farm is in central Illinois (40.06° N, 88.19°W) and the historic land use is corn-soy agriculture (Cheng et al., 2020; Blanc-Betes et al., 2020). In the spring of 2016, a pilot ERW experimental study was conducted using twenty, 2 x 2 m plots in a field of maize; a field-scale experiment was initiated in 2017. This large-scale field experiment consists of several ERW experimental plots of 3.8  
265 ha (200x200 m) each in size, with control and basalt-treated plots, each instrumented with an eddy covariance system at the centre of the plot to measure surface energy, water, and carbon fluxes (Zeri et al., 2011). Soil pH is measured through surface soil samples (0–10 and 10–30 cm) and N<sub>2</sub>O fluxes were monitored through static chambers atop PVC collars during the planting season (Blanc-Betes et al., 2020).

We also compared our global simulation results with available observations and emission inventories. Simulated CLM5  
270 nitrogen emissions are compared with multiple emission inventories, including the Copernicus Atmosphere Monitoring Service (CAMS; Bennouna et al., 2020), Community Emissions Data System (CEDS; Hoesly et al., 2018), Emission Database for Global Atmospheric Research (EDGAR; Crippa et al., 2018) and Harmonized Emissions Component (HEMCO; Lin et al., 2021). For N<sub>2</sub>O, we also used results from the global N<sub>2</sub>O Model Intercomparison Project (NMIP; Tian et al., 2018), and estimates from Wang et al., (2020) and the CarbonTracker Lagrange North American Regional Inversion Framework (Nevison  
275 et al., 2018). Details of all these datasets are presented in Table 1. The datasets were regridded to match our model resolution of 0.9 by 1.25 using bilinear interpolation. It is important to note that our CLM5 model-inventory comparison should be considered as an approximation because our simulations do not match the meteorological years of the inventories and because actual manure and synthetic fertilizer usage in CLM5 may differ from what was assumed in the inventories.

280

**Table 1. Summary of observations and emission inventories used in this study for model comparison and validation.**

<b>Name and Reference</b>	<b>Coverage</b>	<b>Resolution</b>	<b>Period</b>	<b>Notes</b>
CAMS (Granier et al., 2018)	Global	0.1° x 0.1° Monthly	2010–2019	NO and NH <sub>3</sub> from agricultural soils and nitrogen deposition
CEDS (Hoesly et al., 2018)	Global	0.01° x 0.01° Monthly	2005–2015	NO and NH <sub>3</sub> from agricultural soils with both synthetic and manure fertilizers
EDGAR (Crippa et al., 2018)	Global	0.1° x 0.1° Monthly	2010	N <sub>2</sub> O, NO, NH <sub>3</sub> from agricultural soils with both synthetic and manure fertilizers
HEMCO (Lin et al., 2021)	Global	0.5° x 0.625° Monthly	2005–2017	NO soil emissions weighted by CLM5 gridded crop area
NMIP (Tian et al., 2018)	Global	0.5° x 0.5° Annual & Monthly	2000–2015	Modeled N <sub>2</sub> O fluxes in crops from the global N <sub>2</sub> O Model Intercomparison Project
Wang et al., (2020)	Global	0.1° x 0.1° Annual	2010–2014	Modeled N <sub>2</sub> O fluxes in crops with an empirical upscaling method using site-level observations spatially distributed
Nevison et al., (2018)	USA	1° x 1° Daily	2008–2015	N <sub>2</sub> O fluxes from an inversed model with atmospheric N <sub>2</sub> O observations

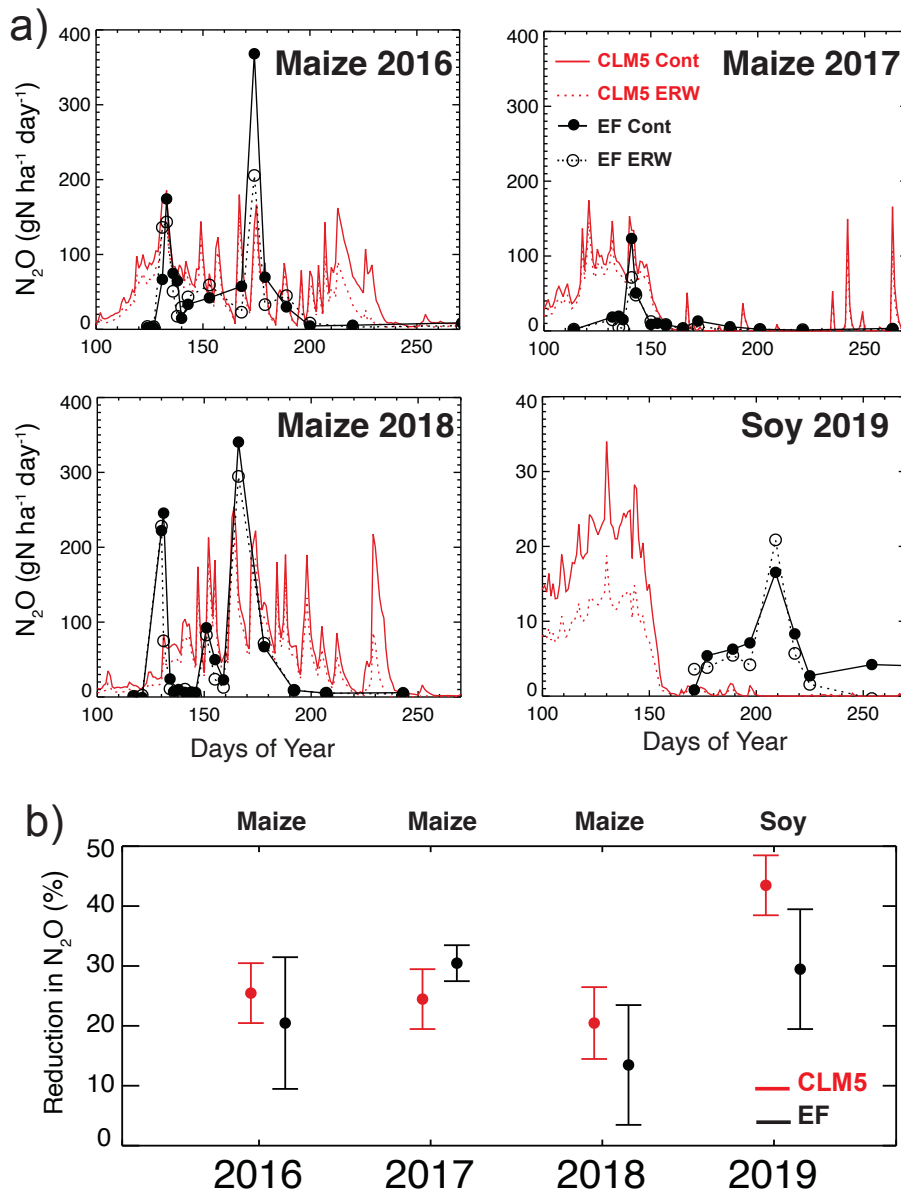
### 3 Validation

285 CLM5 simulations have been extensively evaluated by comparison with observations on a global scale (e.g., Lawrence et al., 2019; Lombardozzi et al., 2020; Nevison et al., 2022b) as well as in specific field sites (e.g., Chen et al., 2020, Nevison et al., 2022a). We focus our evaluation on soil N<sub>2</sub>O fluxes from croplands at the Energy Farm, continental U.S., and agriculture N<sub>2</sub>O, NO<sub>x</sub> and NH<sub>3</sub> emissions at a global scale and the response of the simulated soil N<sub>2</sub>O to changes in soil pH from basalt applications.

### 3.1 Soil N<sub>2</sub>O at the Energy Farm and continental U.S.

Figure 3 compares modeled soil N<sub>2</sub>O in our single-point simulations with available observations at the Energy Farm pre-trail (maize) in 2016 and trial rotation crops (maize, maize, and soybean) in 2017–2019, for control and basalt-treated plots. For daily soil N<sub>2</sub>O fluxes (Fig. 3a), we found that simulated daily N<sub>2</sub>O showed generally good agreement with the limited daily observations at the Energy Farm, simulating larger averaged soil N<sub>2</sub>O fluxes during the growing season in maize (37.2–51.7 gN ha<sup>-1</sup> day<sup>-1</sup>) than soybean (5.4 gN ha<sup>-1</sup> day<sup>-1</sup>), similar to what was observed in the field trails (18.8–62.3 gN ha<sup>-1</sup> day<sup>-1</sup> for maize and 6.2 gN ha<sup>-1</sup> day<sup>-1</sup> for soybean). As shown for DAYCENT by Blanc-Betes et al., (2020), CLM5 also simulates well the increases in N<sub>2</sub>O fluxes following fertilization and precipitation events at the Energy Farm, although with daily fluxes peaking slightly earlier in the growing season compared to observations due to yearly differences in planting schedule and fertilization. We note that in this project CLM5 has not been tuned specifically for the Energy Farm conditions or across the U.S., rather used as in the released version as the objective is to use the model at a global scale, across many crops, regions and for future climate projections. As a result, the land management practices, such as planting and harvesting times, as well as fertilizer application frequency and rates, employed in our simulations may not precisely match those implemented at the Energy Farm. To facilitate a more direct comparison for soybean, we made an exception and turned off synthetic and manure fertilizers in the soybean simulation because the Energy Farm does not apply nitrogen fertilizers to this crop.

To determine if CLM5 simulates soil N<sub>2</sub>O changes due to basalt amendments, we compared the relative changes in N<sub>2</sub>O in the basalt-treated plots with respect to the control plots for each year, at the Energy Farm and simulated by the model in Fig. 3b. The changes in N<sub>2</sub>O were obtained by comparing the cumulative N<sub>2</sub>O at the end of the growing season using the measured and simulated N<sub>2</sub>O flux at the time of the discrete measurements. For the basalt amendment run in CLM5, we considered the same increases in soil pH observed in the field experiments (section 2.3; Blanc-Betes et al., 2020). We found that CLM5 effectively reproduces the decrease in soil N<sub>2</sub>O in the basalt-treated plots with soil N<sub>2</sub>O fluxes 21–25% (maize) and 44% (soy) smaller than control plots, in line with the observed decreases of 12–32% and 31% at the Energy Farm.



315 **Figure 3: Soil N<sub>2</sub>O fluxes at the Energy Farm for the pilot study (maize; 2016) and the large field trials (rotation crops**  
**as maize, maize and soybean; 2017–2019). Shown is simulated (red) and observed (black) daily N<sub>2</sub>O fluxes (g N ha<sup>-1</sup>**  
**day<sup>-1</sup>) at the control (solid lines or solid circles) and basalt-treated plots (dotted lines or open circles) (a) and reductions**  
**in N<sub>2</sub>O emissions (%) in the basalt-treated plots compared to the control plots for the simulated by CLM5 (red) and**  
**measured at the field experiments (black) (b). Error bars represent variability in the reduction (%) estimated using**  
 320 **propagation of errors.**

We used observations of N<sub>2</sub>O from agricultural fields summarized in published studies (e.g., Stehfest and Bouwman, 2006; Shcherbak et al., 2014; Wang et al., 2018), including the Energy Farm, and N<sub>2</sub>O emissions estimated across North America using the Carbon Tracker-Lagrange regional inversion framework (Nevison et al., 2018) to assess how well CLM5 captures agriculture N<sub>2</sub>O emissions in the U.S., an important agricultural region suitable for large-scale ERW deployment (Beerling et al., 2020) (Fig. 4).

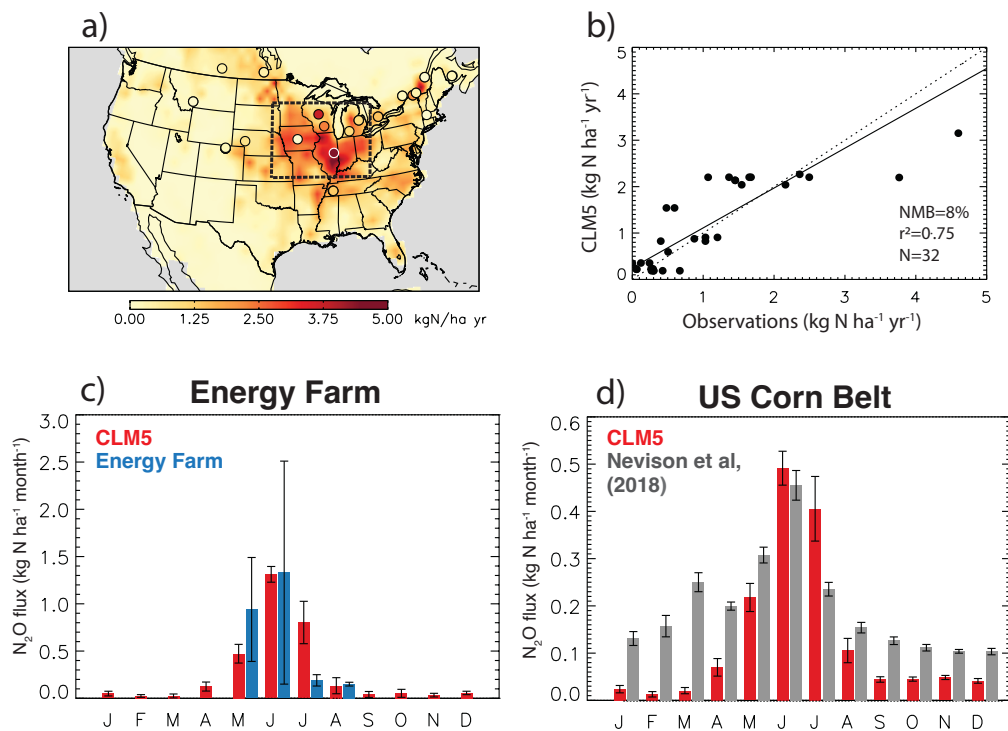


**Figure 4: Soil N<sub>2</sub>O fluxes in U.S. with modelled and observed values at individual measurement sites (a), the scatter plot with modelled and observed values at the individual sites (b), seasonal variability of monthly soil N<sub>2</sub>O at the location of the Energy Farm (c) and across the US Corn Belt (d). Observations are means from published measurements, including the Energy Farm (2017-2019; Blanc-Betes et al., 2021) or averaged monthly fluxes from the Carbon Tracker-Lagrange regional inversion model (2008-2014; Nevison et al., 2018). The squared-correlation coefficient ( $r^2$ ), nominal mean bias (NMB, %) and number of observations (N) are shown in the inset. Reduced major axis-regression lines (solid) for croplands and the 1:1 line (dashed) are also shown. The US Corn Belt is represented with a dashed box and location of Energy Farm (40.07 N, 88.2 W) with a white border circle in the CLM5 map. Error bars represent the standard deviation of the annual totals.**

For our studied period, CLM5 estimates a total N<sub>2</sub>O emission across continental U.S. croplands of  $0.59 \pm 0.06$  Tg N<sub>2</sub>O-N yr<sup>-1</sup>, with more than 50% emitted in the U.S. Corn Belt. Our soil N<sub>2</sub>O emissions fall well within the range of previous estimates for direct agriculture emissions in the U.S. (0.3–1.1 Tg N yr<sup>-1</sup>) reported by the U.S. Environmental Protection Agency (EPA),

bottom-up inventories, and other processed-based land models (e.g., Tian et al., 2019; Lu et al., 2021; U.S. EPA, 2022). Similar  
340 to other studies, our modelled estimates are lower than those reported from top-down N<sub>2</sub>O studies (1.6–2.6 Tg N yr<sup>-1</sup>; Miller  
et al., 2012; Nevison et al., 2018) as they consider more N<sub>2</sub>O source types than direct agriculture emissions, e.g., fossil fuel  
combustion, industry non-combustion processes, biomass burning, and solid waste and sewage water. For the U.S. Corn Belt,  
dominated by agriculture sources, our annual flux (0.31±0.04 Tg N<sub>2</sub>O- N yr<sup>-1</sup>) is comparable to that from top-down estimates  
(0.32–0.42 Tg N yr<sup>-1</sup>; Griffins et al., 2013; Chen et al., 2016; Nevison et al., 2018) as well as previous estimates with process-  
345 based models (0.26–0.60 Tg N yr<sup>-1</sup> (e.g., Li et al., 1996; Del Grosso et al., 2006; Lu et al., 2021).

We synthesized a consistent set of field observations representative of long-term means for different croplands across North  
America and identified a total of 32 observations gathered from 1998 to 2016 (Figs. 4a-b). We summarized the comparison  
between the model and observations using the normalized mean bias ( $NMB = \frac{\sum(M_i - O_i)}{\sum O_i}$ , where  $M_i$  and  $O_i$  are modelled and  
observed) and the squared-correlation coefficient ( $r^2$ ). We found that the model captures well the spatial distribution of soil  
350 N<sub>2</sub>O in croplands across the U.S.. Simulated soil N<sub>2</sub>O fluxes show good agreement with the mean observations over croplands  
( $r^2=0.75$ ) although they are slightly overestimated (NMB=8%).

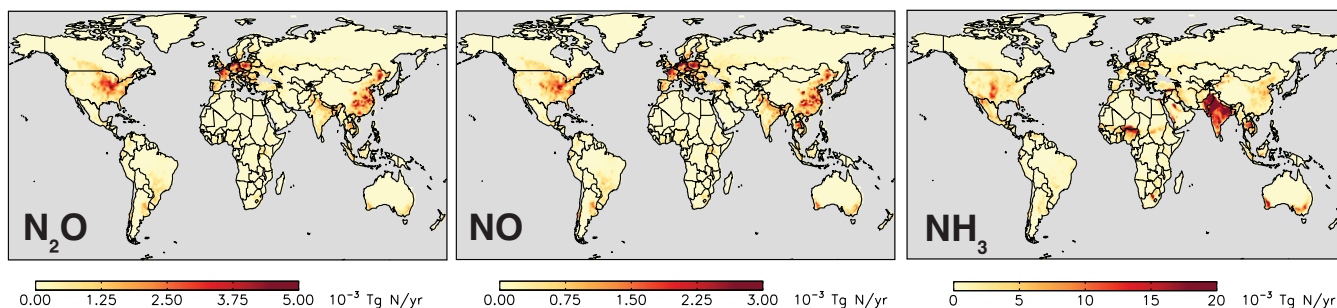
We also evaluated the seasonal variability of our simulated soil agriculture N<sub>2</sub>O fluxes in the U.S. (Figs. 4c-d) using averaged  
field observations at the Energy Farm (Blanc-Betes et al., 2020) and regionally averaged monthly fluxes in the Corn Belt from  
the Carbon Tracker-Lagrange regional inversion framework (Nevison et al., 2018). Figure 4a shows the location of the Energy  
355 Farm and the approximate limits of the U.S. Corn Belt. We found that the model represents reasonably well the seasonal  
variability of soil N<sub>2</sub>O fluxes across the Corn Belt as well as at the Energy Farm in Illinois, with direct agriculture N<sub>2</sub>O  
emissions peaking up early in the growing season (April–May), which coincides with addition of fertilization, as in the  
observations.

### 3.2 Global soil NO, N<sub>2</sub>O and NH<sub>3</sub>

360 We also evaluated soil NO, N<sub>2</sub>O and NH<sub>3</sub> emissions simulated by CLM5 in the global control simulation. Figure 5 presents  
the total annual global N<sub>2</sub>O, NO and NH<sub>3</sub> agriculture emissions averaged over 5 years (2010–2014) in our simulations. Soil  
NO and NH<sub>3</sub> emissions are at above-canopy (sections 2.2.2 and 2.2.3). We also compared our soil gas nitrogen emissions with  
the available estimates reported in a wide range of global emission inventories (CAM5, CEDS, EDGAR, HEMCO) and  
previously modeled agriculture fluxes (NMIP, Tian et al., 2018 and Wang et al., 2020) (Table 1). NH<sub>3</sub> emissions were  
365 extensively evaluated in Fung et al., (2020) and we included here a follow-up and simpler validation to assess our small updates  
in the parameterization (section 2.3.3).

Emission inventories provide monthly estimates from several agriculture sources, such as synthetic and organic fertilizers,  
manure management, indirect nitrogen losses, among others and, in some cases, emissions from soils in natural ecosystems.  
To be able to compare the emissions directly with the CLM5 estimates, we extracted monthly emission estimates and selected

370 the sources to represent as best as possible direct agriculture emissions from synthetic and manure fertilizers. In the case of HEMCO, which provides soil NO emissions from both natural and agricultural soils, we weighted their emissions by the fraction of cropland covering each grid-cell in CLM5. For NH<sub>3</sub>, we considered that one-third of the total agricultural NH<sub>3</sub> emission reported by CAMS, CEDS and EDGAR is attributed to fertilizers, which aligns with the fraction reported in previous studies and environmental assessments (e.g., Paulot et al., 2014; National European Environment Agency, 2013; Fung et al., 375 2022). We conducted a spatial comparison of the annual N<sub>2</sub>O, NO and NH<sub>3</sub> emissions from CLM5 and each inventory (grid-cell by grid-cell) by computing the normalized mean bias (NMB) and the Pearson’s correlation coefficient (*r*). Table 2 shows the annual totals and a summary of these statistics. Spatial distribution of annual-total N<sub>2</sub>O emission estimated by the inventories and differences with CLM5 are shown in Figs. S6–S8 in SM.



380 **Figure 5: Simulated global soil agriculture N<sub>2</sub>O, NO and NH<sub>3</sub> emissions in CLM5 without basalt (‘Control Run’).**

**Table 2. Summary of agriculture N<sub>2</sub>O, NO and NH<sub>3</sub> fluxes. Reported is the total global emission (average ± standard deviation of the annual totals), nominal mean bias (NMB) and Pearson’s correlation coefficient (*r*).**

Emissions	N <sub>2</sub> O			NO			NH <sub>3</sub>		
	Total (Tg N yr <sup>-1</sup> )	NMB (%)	<i>r</i>	Total (Tg N yr <sup>-1</sup> )	NMB (%)	<i>r</i>	Total (Tg N yr <sup>-1</sup> )	NMB (%)	<i>r</i>
CLM5	3.12±0.12	–	–	2.17±0.06	–	–	15.18±0.39	–	–
CAMS	–	–	–	2.05±0.02	6	0.6	11.78±0.40	38	0.5
CEDS	–	–	–	1.38±0.06	57	0.4	11.40±0.30	34	0.6
EDGAR <sup>a</sup>	3.03	3	0.3	1.00	117	0.4	10.3	46	0.5
HEMCO	–	–	–	2.27±0.10	-5	0.4	–	–	–
NMIP	3.30±1.20 <sup>b</sup>	-7	0.4	–	–	–	–	–	–
Wang et al.,	2.56±0.03	22	0.3	–	–	–	–	–	–

<sup>a</sup>Only monthly data are available for 2010. Reported mean of 2010.

385 <sup>b</sup>Reported mean ± standard deviation of seven models



For N<sub>2</sub>O, CLM5 estimates global direct agriculture emissions of 3.1 Tg N<sub>2</sub>O-N yr<sup>-1</sup>, which is in line with previous annual estimates for agriculture sources (1.7–5.8 Tg N yr<sup>-1</sup>; e.g., Del Grosso et al., 2006; Syakila and Kroeze, 2011; Saikawa et al., 2014) and the IPCC 2021 reported values for 2007–2016 (3.8 Tg N yr<sup>-1</sup>) (Canadell et al., 2021). Our estimate is similar to the  
390 widely used EDGAR emission inventory (3.03 Tg N yr<sup>-1</sup>) and falls within the range of modeled estimates (2.6–3.3 Tg N yr<sup>-1</sup>; Tian et al., 2018; Wang et al., 2020). The global *r* values range between 0.3 and 0.4 across the inventory and models, suggesting that CLM5 does not exactly replicate the spatial patterns reported on the emission inventories. The global NMB values are small and range between -7 to 25%, showing a good agreement with the reported estimates overall.

For global agriculture NO emissions, CLM5 estimates 2.2 Tg NO-N yr<sup>-1</sup>, which is in line with previously reported fertilizer-  
395 induced soil NO emissions (0.4–3.5 Tg N yr<sup>-1</sup> e.g., Stehfest and Bouwman, 2006; Crippa et al., 2018; Bennouna et al., 2020; Lin et al., 2021). Our global *r* values lie between 0.4–0.6 across all inventories, indicating a fair correlation. Our estimate is higher than two emission inventories (CEDS and EDGAR) with a global NMB value between 57 and 117%, but close to the CAMS (NMB=6%) and the adjusted HEMCO (NMB=-5%) estimates.

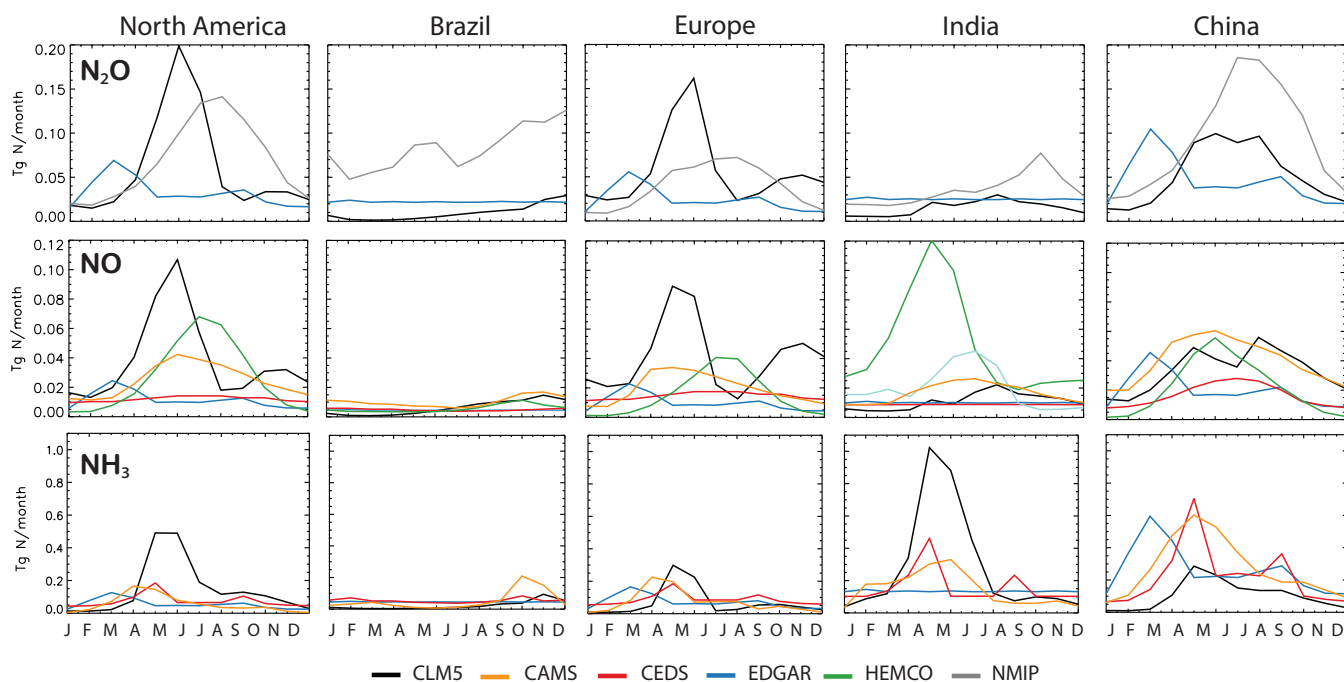
Global fertilizer-induced NH<sub>3</sub> emissions in CLM5 are 15.2 Tg NH<sub>3</sub>-N yr<sup>-1</sup>. This estimate is close to estimates (from synthetic  
400 and manure fertilizers) reported by Fung et al., (2020) (14 Tg N yr<sup>-1</sup>) and Vira et al., (2020) (18 Tg N yr<sup>-1</sup>) for NH<sub>3</sub> schemes also implemented in CLM5. It is important to note that despite using Fung et al., (2020) NH<sub>3</sub> parameterization in CLM5, our estimate is not exactly as that work because we updated the nitrification and denitrification schemes as well as implemented a dependance on soil pH (section 2.2.3). As indicated by Fung et al., (2020), the CLM5 estimates are slightly higher than three widely used global emissions inventories (10–12 Tg N yr<sup>-1</sup>; CAMS, CEDS and EDGAR). The global *r* values are 0.5–0.6,  
405 indicating a fair correlation between CLM5 in all three emission inventories. The high bias in CLM5 is indicated by global NMB values of approximately 34–46% between CLM5 and the emission inventories.

In CLM5 as well as other models and emission inventories, the largest agricultural emissions are found over major cropland regions (Fig. 5 and Figs. S6-S8). However, their spatial distribution differs mostly due to differences in fertilization rates and application patterns adopted by the models and emission inventories and in some cases, spatial distribution of soil pH. Table  
410 3 summarizes the regional emission totals in our five studied agricultural regions. These areas are major food-producing regions and are responsible for most of the agriculture N<sub>2</sub>O (75%), NO (61%) and NH<sub>3</sub> (55%) emissions with respect to the global total. In CLM5, major crop N<sub>2</sub>O emitters are Europe (0.68 Tg N yr<sup>-1</sup>), China (0.63 Tg N yr<sup>-1</sup>) and North America (0.59 Tg N yr<sup>-1</sup>), each with about 19–22% of global emissions. Soil NO losses are similar, with Europe (0.49 Tg N yr<sup>-1</sup>; 23%), North America (0.37 Tg N yr<sup>-1</sup>; 17%), and China (0.40 Tg N yr<sup>-1</sup>; 18%) as the largest agriculture sources. As reported by Fung et al  
415 (2020), major fertilizer-induced NH<sub>3</sub> emissions in CLM5 are from India (3.47 Tg N yr<sup>-1</sup>; 23%), followed by North America (1.77 Tg N yr<sup>-1</sup>; 12%) and China (1.25 Tg N yr<sup>-1</sup>; 8%). Emission inventories show a similar regional distribution of emissions, with a higher proportion of agriculture emissions in China and India. For example, for NH<sub>3</sub> emissions, CAMS, CEDS, and EDGAR indicate that India is the largest emitter, accounting for 23–30% of global emissions, followed by China with 16–17%.

420 Figure 6 shows the seasonality of  $\text{N}_2\text{O}$ ,  $\text{NO}$  and  $\text{NH}_3$  emissions in these five main crop regions for CLM5 and global inventories and NMIP. In this analysis, for NMIP  $\text{N}_2\text{O}$  fluxes we considered the average of only two models as not all seven provided monthly outputs (Hanqin Tian, Auburn University, personal communication, 2019). In CLM5, each crop has fertilizer applied (as  $\text{NH}_4^+$ ) evenly over the course of 20 days beginning with leaf emergence (section 2.1). The addition of  $\text{NH}_4^+$  in the soil accelerates plant uptake, microbial immobilization, denitrification, nitrification and  $\text{NH}_3$  volatilization, which explains why

425  $\text{N}_2\text{O}$ ,  $\text{NO}$  and  $\text{NH}_3$  emissions peak mostly in spring (March–May) in North America, Europe, China and India and in the fall (October–November) in Brazil. Soil  $\text{N}_2\text{O}$  and  $\text{NO}$  fluxes are also strongly dependent on environmental conditions (e.g., precipitation), which mainly drive the smaller secondary peaks later in the season in North America, Europe and China. All global emission inventories and NMIP estimates show similar emission variability, with springtime peaks in the Northern hemisphere (North America, Europe, China, and India) and fall peaks in the southern hemisphere (Brazil). For soil  $\text{N}_2\text{O}$ , the

430 seasonality in CLM5 is consistent with that given by the NMIP models although significantly lower in magnitude for Brazil and China. However, annual estimates in CLM5 for Brazil ( $0.12 \text{ Tg N yr}^{-1}$ ) and China ( $0.63 \text{ Tg N yr}^{-1}$ ) are in line with the average from the seven-model ensemble ( $0.20 \text{ Tg N yr}^{-1}$  and  $0.80 \text{ Tg N yr}^{-1}$ , respectively) (Table 3).



435 **Figure 6: Monthly agriculture  $\text{N}_2\text{O}$ ,  $\text{NO}$  and  $\text{NH}_3$  emissions in the main crop regions considered in the study (North America, Brazil, Europe, India, and China) estimated by CLM5, CAMS, CEDS, EDGAR, HEMCO and NMIP (Table 1). Soil  $\text{NO}$  emissions in HEMCO were weighted by cropland fraction; soil  $\text{N}_2\text{O}$  in NMIP is the average of only two models that provided monthly output.**

**Table 3. Summary of regional agriculture N<sub>2</sub>O, NO and NH<sub>3</sub> fluxes in CLM5 and emission inventories.**

<b>Emissions</b>	<b>North America</b>	<b>Brazil</b>	<b>Europe</b>	<b>India</b>	<b>China</b>
<b>N<sub>2</sub>O (Tg N yr<sup>-1</sup>)</b>					
CLM5	0.59	0.12	0.68	0.18	0.63
EDGAR	0.30	0.27	0.29	0.30	0.55
NMIP	0.30	0.20	0.30	0.50	0.80
<b>NO (Tg N yr<sup>-1</sup>)</b>					
CLM5	0.37	0.07	0.49	0.13	0.40
CAMS	0.12	0.20	0.15	0.24	0.25
CEDS	0.11	0.06	0.17	0.11	0.20
EDGAR	0.10	0.05	0.12	0.12	0.24
HEMCO	0.25	0.07	0.18	0.58	0.26
<b>NH<sub>3</sub> (Tg N yr<sup>-1</sup>)</b>					
CLM5	1.77	0.26	0.82	3.47	1.25
CAMS	0.66	0.63	0.86	1.76	3.24
CEDS	0.88	0.64	1.04	1.89	2.61
EDGAR	0.66	0.55	0.86	1.61	3.11

It is important to acknowledge that substantial differences among emission inventories also exist in terms of their magnitude, spatial distribution and seasonality. For example, soil N<sub>2</sub>O, NO and NH<sub>3</sub> emissions in EDGAR always peak about one month earlier in the season than the other emission inventories and CLM5; soil NH<sub>3</sub> emissions in CEDS have two seasonal peaks compared to CAMS, CLM5 and EDGAR. As discussed by Fung et al., (2020), these disparities are primarily caused by differences in the planting season and length of fertilization considered within the inventories as well as the agriculture sources included (e.g., synthetic and/or manure application, manure management, etc). In addition, there are systematic uncertainties in the global inventories (e.g., emission factors, environmental conditions, fertilizer types and rates, etc) (Hoesly et al., 2018; Fung et al., 2020). Here we did not intend to understand these differences, rather use the model-inventory comparison to assess the CLM5 performance. We concluded that CLM5 provides a reasonable representation of the magnitude and seasonality of direct agriculture nitrogen emissions across the major hotspot regions (North America, Brazil, Europe, India, and China),

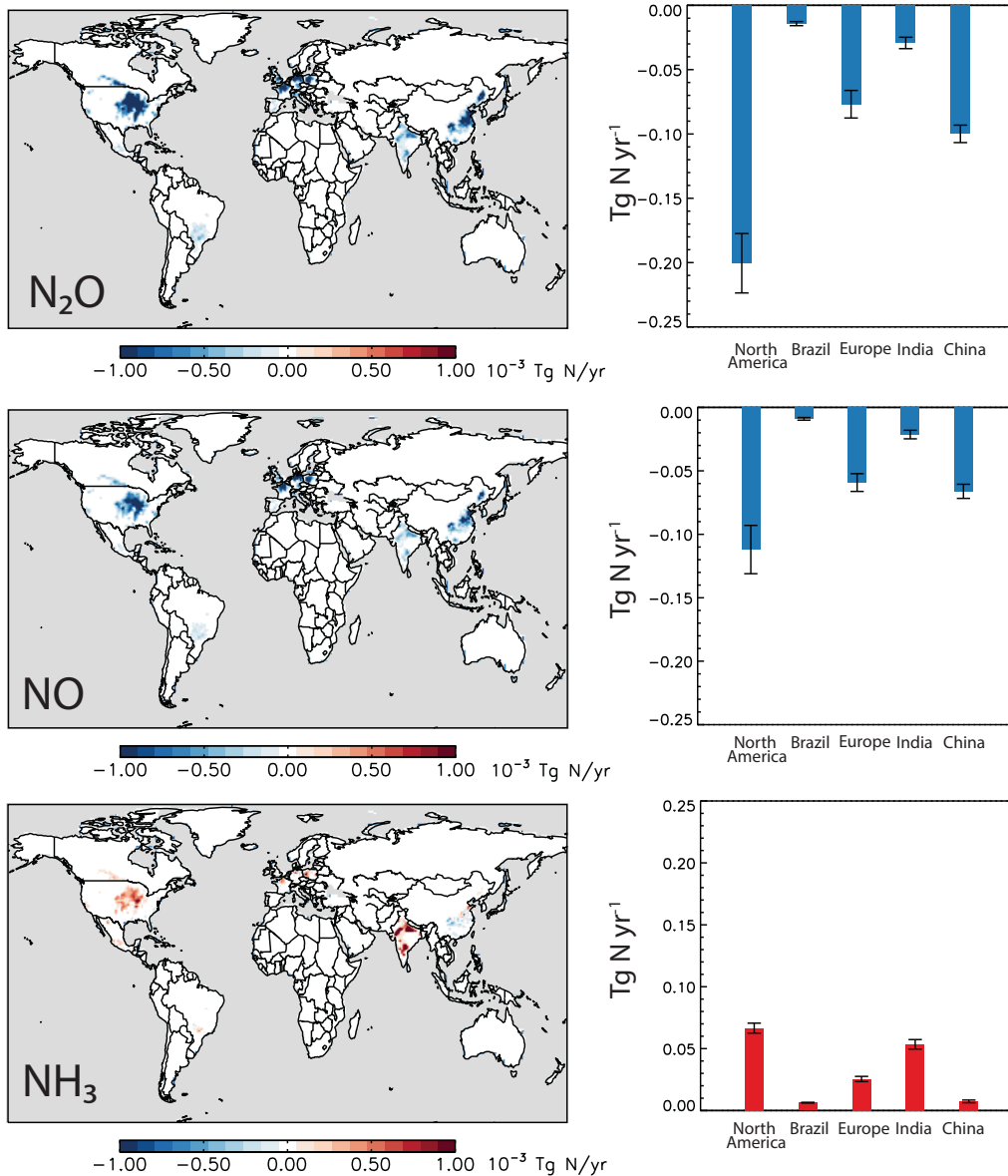
which are relevant for our study. We note that there may be some limitations and uncertainties associated with the model's performance as well as current emission inventories in capturing the full complexity of these emissions. Further investigations and validation efforts are warranted to enhance our understanding of regional variations in agricultural nitrogen emissions.

#### 4 Effect of basalt application on soil nitrogen gas emissions

We assessed the regional impact of amending cropland soils with basalt by estimating changes in the nitrogen cycling. We performed this case study by using the soil pH increases after 25 years of repeated annual basalt application as well as optimized deployment locations required to remove 2Gt CO<sub>2</sub> yr<sup>-1</sup> projected by the ERW Model in Beerling et al., (2020) (Figs. 2 and S5). Figure 7 shows the changes in soil N<sub>2</sub>O, NO and NH<sub>3</sub> emissions due to large-scale deployment of ERW with croplands and summarizes the regional changes across the five agricultural regions (North America, Brazil, Europe, India, and China). A close-up view of changes in these five regions are included in Fig. S9 in SM; regional emissions in the Control and ERW runs are summarized in Table 4.

**Table 4. Soil N<sub>2</sub>O, NO and NH<sub>3</sub> fluxes in the control and basalt treatment CLM5 runs on main cropland regions. Reported is total emission as average ± standard deviation of the annual totals.**

Region	N <sub>2</sub> O (Tg N yr <sup>-1</sup> )		NO (Tg N yr <sup>-1</sup> )		NH <sub>3</sub> (Tg N yr <sup>-1</sup> )	
	Control	ERW	Control	ERW	Control	ERW
North America	0.59±0.06	0.40±0.03	0.37±0.04	0.27±0.03	1.77±0.25	1.83±0.25
Brazil	0.12±0.01	0.10±0.01	0.07±0.01	0.07±0.01	0.26±0.03	0.27±0.03
Europe	0.68±0.06	0.60±0.05	0.49±0.04	0.43±0.03	0.82±0.05	0.85±0.06
India	0.18±0.02	0.15±0.02	0.13±0.02	0.11±0.01	3.47±0.29	3.53±0.29
China	0.63±0.03	0.53±0.02	0.40±0.02	0.33±0.01	1.25±0.04	1.26±0.04
Total	2.20±0.09	1.78±0.07	1.46±0.06	1.21±0.05	7.57±0.38	7.74±0.39



470

**Figure 7: Changes in annual soil  $N_2O$ ,  $NO$  and  $NH_3$  fluxes across the main five agriculture regions (North America, Brazil, Europe, India, and China) based on increases in soil pH resulting from basalt treatment required to sequester  $2 \text{ Gt CO}_2 \text{ yr}^{-1}$  (Figure 2). Shown is the spatial distribution of changes in soil  $N_2O$ ,  $NO$  and  $NH_3$  ( $\Delta \text{ERW-Control}$ ) and the summary of the regional changes ( $\text{Tg N yr}^{-1}$ ). Error bars indicate the standard deviation of the annual total changes.**

475

Large-scale basalt application consistently decreases soil  $N_2O$  and  $NO$  emissions over the five main agriculture regions, with a total decrease of  $0.42 \text{ Tg N}_2\text{O-N yr}^{-1}$  and  $0.25 \text{ Tg NO-N yr}^{-1}$ . These changes are substantial and correspond to 19% for  $N_2O$

and 17% for NO of the total agricultural emissions in those five regions, with 13% for N<sub>2</sub>O, and 12% for NO of the global total. Major reductions in N<sub>2</sub>O and NO occurred in North America (28% for N<sub>2</sub>O and 24% for NO), followed by China (16% and 18%) and Europe (13% and 12%).

Our new modeling framework only simulates changes in direct soil N<sub>2</sub>O emissions in croplands. Indirect soil nitrogen emissions occur through degassing of N<sub>2</sub>O from aquifers and surface waters, via the leaching and runoff of applied N (NO<sub>3</sub> and NH<sub>4</sub>) in aquatic systems, and the volatilisation of applied N as NH<sub>3</sub> and NO<sub>x</sub> followed by deposition of NH<sub>4</sub> and NO<sub>x</sub> on soils and water (Nevison, 2021). ERW field trials in the U.S. have reported nitrogen losses (in the form of NO<sub>3</sub> and NH<sub>4</sub>) to leaching in the basalt-treated plots that are substantially larger than the control plots in maize (40%) and miscanthus (17%) (Blanc-Betes et al., 2020). However, this indirect contribution to the overall emissions is expected to be small, given that indirect emissions account for less than 5% of total agricultural N<sub>2</sub>O emissions (Nevison, 2021; Lu et al., 2022).

Basalt applications increased soil NH<sub>3</sub> emissions as expected, with a total increase of 0.17 Tg NH<sub>3</sub>-N yr<sup>-1</sup>, which is about 2% of agriculture emissions in our five regions and 1% of the global total. The increasing effect on NH<sub>3</sub> is not as consistent across all soils as for N<sub>2</sub>O and NO and some grid cells with acidic soils (pH < 5.5) displayed decreases in NH<sub>3</sub>, especially in regions across Brazil and China (Fig. S8). Increases in soil pH favours nitrification and subsequent denitrification processes (Parton et al., 1996), which reduces N in the NH<sub>4</sub><sup>+</sup> form in the soils available for NH<sub>3</sub> volatilization. Overall, relatively major increases in NH<sub>3</sub> occurred in North America, Brazil and Europe (3–4%), followed by India (1.5%) with marginal increases in China (0.8%). Regions with more neutral and alkaline soils have more significant increases (8–12%), such as croplands in the U.S. with soil pH ranging 6.5–7.5, which showed increases up to 10%.

## 5 Conclusions

We present the development and implementation of new updates and schemes for the CLM5 nitrogen cycle to evaluate the potential impact of ERW with croplands. In particular, new updates in N<sub>2</sub>O focus on the gross denitrification and denitrification end products rates described by Blanc-Betes et al., (2020) based on observations on ERW field trials in the US, and the N<sub>2</sub>O nitrification rate. In addition, we implement a new parameterization to calculate NO release from nitrification and denitrification processes, considering rain pulses in nitrification and losses of NO to plant canopy. Finally, for NH<sub>3</sub> we use the volatilization scheme (Fu et al., 2020), with a regulating pH function based on observations of basalt, lime, and biochar applications.

Using our global simulations, we successfully validated simulated ‘control’ (i.e., no ERW) seasonal cycles of soil N<sub>2</sub>O, NO and NH<sub>3</sub> emissions against a wide range of global emission inventories and previously reported estimates. For N<sub>2</sub>O, we also use results from the N<sub>2</sub>O Model Intercomparison Project, the Carbon-Tracker Lagrange North American Regional Inversion Framework and a compilation of long-term observations in different croplands across North America. We also benchmarked simulated mitigation of soil N<sub>2</sub>O fluxes in response to ERW against a sub-set of data from ERW field trials in the U.S. Corn

510 Belt with single-point simulations at Energy Farm in Illinois (U.S.) and provide a case study of the effect of large-scale ERW deployment with croplands on soil nitrogen fluxes across five key regions with high potential for CDR with ERW (North America, Brazil, Europe, India, and China).

We acknowledge the need for further improvement in the CLM5 nitrogen cycling representation and the ERW parameterization. In a comprehensive evaluation of CLM5 nitrification and denitrification processes, Nevison et al. (2022b) emphasized that the nitrification:denitrification ratio (2:1) in CLM5 is likely to be unrealistically low, even when considering 515 the missing N mineralization term in potential nitrification (Section 2.2.1). Consequently, CLM5 underestimates the fraction of gross mineralization leading to nitrification and overestimates  $\text{NH}_4^+$  uptake by plants. Additionally, CLM5 underestimates  $\text{NO}_3$  assimilation by immobilizing bacteria. To enhance the confidence in our land model simulations, it is thus crucial to gather more experimental data from ERW field trials as well as observational constraints on soil nitrogen fluxes and flux ratios.

Our study represents a first implementation of an ERW parametrization in a land model N cycling, which has enabled us to 520 understand the implication of large-scale deployment of ERW with croplands on direct soil nitrogen trace gas emissions. Our modelling framework simulates important reductions in both  $\text{N}_2\text{O}$  (19%) and  $\text{NO}$  (17%) and moderate increases in  $\text{NH}_3$  (2%) across five main cropland regions, using the soil pH increases that would occur after 25-year basalt application to remove 2Gt  $\text{CO}_2$  per year projected (Beerling et al., 2020). Reductions are most marked over North America, with decreases of 28% in  $\text{N}_2\text{O}$  and 24% in  $\text{NO}$  and increases of about 10% in  $\text{NH}_3$  (for neutral and alkaline agriculture soils).

525 Given agricultural  $\text{N}_2\text{O}$  emissions account for more than 50% of the total  $\text{N}_2\text{O}$  emissions (Tian et al., 2020) and these emissions are expected to continue to grow due to increases in fertilizer usage (IPCC, 2021), regional decreases in  $\text{N}_2\text{O}$  emissions from basalt amendments in croplands are significant and may impact stratospheric ozone. Our study highlights the additional potential of ERW for climate change mitigation through reducing emissions of a non- $\text{CO}_2$  greenhouse gas.

530 Simulated decreases in soil  $\text{NO}$  emissions and moderate increases in  $\text{NH}_3$  from basalt treatments in our five cropland regions has further implications for regional air quality. Once emitted from soil,  $\text{NH}_3$  undergoes rapid reactions in the atmosphere forming inorganic  $\text{NO}_3^-$  and  $\text{NH}_4^+$  aerosols, which contributes to  $\text{PM}_{2.5}$  formation. Agriculture  $\text{NH}_3$  emissions are responsible for 30% of all  $\text{PM}_{2.5}$  in the U.S., 50% in Europe and 20% in China (e.g., Wyer et al., 2022). Similarly, soil  $\text{NO}$  is rapidly oxidized, generating tropospheric  $\text{O}_3$  and secondary organic aerosols (SOA). Ozone is a strong oxidant, which causes harm to human health and to crops, and SOA also contributes to  $\text{PM}_{2.5}$ . These past decades, significant government attention has been 535 focused on regulating  $\text{NH}_3$  emissions as a strategy for reducing  $\text{PM}_{2.5}$  (e.g., U.S. EPA, 2004; UK DEFRA, 2019). However, in future emission projections, it is unclear whether controlling  $\text{NH}_3$  may be an effective strategy for reducing  $\text{PM}_{2.5}$  particularly given that  $\text{NO}_x$  can also act as the primary limiting precursor for the formation of secondary  $\text{NH}_4^+$  aerosols (e.g., Vieno et al., 2016). Our study thus provides a scientific modelling tool to aid stakeholders in evaluating global and regional ERW proposals as an additional strategy to mitigate climate change and ensuring a clean and sustainable environment.

540 **Code and data availability:** CLM5.0 is publicly available through the Community Terrestrial System Model (CTSM) git

repository (<https://github.com/ESCOMP/ctsm>). Results presented in this paper were obtained using CLM5.0.25 with an updated version of the nitrogen cycling scheme, which is publicly available through the Zenodo repository (<https://doi.org/10.5281/zenodo.8111541>). All emission inventory and published observational data used in the study are available from the provided references. Unpublished soil N<sub>2</sub>O fluxes from the Energy Farm ERW field trials and CLM5 output data and metadata to recreate the analysis are available through the Zenodo repository (<https://doi.org/10.5281/zenodo.8119634>).

**Author contribution:** MVM developed and implemented the new code, performed the modelling experiments, and analyzed the output. EBB, KMF, LLT, LKE, WRW and APKT provided input for the model development. MVM, EK and DJB designed the modelling experiment. IBK, MDM, EHD, IC and NJP provided observations collected in ERW field experiments. MVM prepared the manuscript with contributions from all co-authors.

**Competing interests:** The authors declare that they have no conflict of interest.

**Acknowledgements:** This work was supported by the UKRI Future Leaders Fellowship Programme awarded to MVM (MR/T019867/1) and the Leverhulme Research Centre Award (RC-2015–02) awarded to DJB. Development of NH<sub>3</sub> emission model was supported in part by the General Research Fund (grant no. 14307722) awarded by the Research Grants Council of Hong Kong to APKT. We thank Cynthia Nevison (INSTAAR), Hanqin Tian (Auburn University), Julius Vira (Finnish Meteorological Institute) and Anthony Wong (University of Boston, now MIT) for helpful discussions. High-performance computing support from Cheyenne (doi:10.5065/D6RX99HX) was provided by NCAR’s Computational and Information Systems Laboratory, sponsored by the National Science Foundation under Cooperative Agreement No. 1852977.

## References

- Bakwin, P. S., S. C. Wofsy, S. M. Fan, M. Keller, S. E. Trumbore, and J. M. Da Costa: Emission of nitric oxide from tropical forest soils and exchange of NO between the forest canopy and atmospheric boundary layers, *J. Geophys. Res.*, 95(D10), 16,755–16,764, 1990.
- Blanc-Betes, E, Kantola, IB, Gomez-Casanovas, N, et al.: In silico assessment of the potential of basalt amendments to reduce N<sub>2</sub>O emissions from bioenergy crops. *GCB Bioenergy*, 13: 224–241, <https://doi.org/10.1111/gcbb.12757>, 2020.
- Beerling, D.J., Leake, J.R., Long, S.P., Scholes, J.D., Ton, J., Nelson, P.N., Bird, M.I., Kantzas, E., Taylor, L.L., Sarkar, B., Kelland, M., DeLucia, E., Kantola, I., Müller, C., Rau, G. & Hansen, J.: Farming with crops and rocks to address global climate, food and soil security, *Nature Plants*, 4, 138–147, <https://doi.org/10.1038/s41477-018-0108-y>, 2018.
- Beerling, D.J., Kantzas, E.P., Lomas, M.R. et al.: Potential for large-scale CO<sub>2</sub> removal via enhanced rock weathering with croplands, *Nature*, 583, 242–248, <https://doi.org/10.1038/s41586-020-2448-9>, 2020.
- Bennouna, .Y, Christophe, Y., Schulz, M.Y., Christophe, H.J., Eskes, Basart, S., Benedictow, A.-M., Blechschmidt, S, Chabrillat, C.E., Cuevas, H, Flentje, KM, Hansen, UIM, Kapsomenakis, J, Langerock, B, Petersen, K, Richter, A, Sudarchikova, N, Thouret, V, Wagner, A, Wang, Y, Warneke, T, Zerefos, C.: Validation report of the CAMS global Reanalysis of aerosols and reactive gases, years 2003–2019, Copernicus Atmosphere Monitoring Service (CAMS), <http://dx.doi.org/10.24380/2v3p-ab79>, 2020.



- 575 Canadell, J.G., P.M.S. Monteiro, M.H. Costa, L. Cotrim da Cunha, P.M. Cox, A.V. Eliseev, S. Henson, M. Ishii, S. Jaccard, C. Koven, A. Lohila, P.K. Patra, S. Piao, J. Rogelj, S. Syampungani, S. Zaehle, and K. Zickfeld, 2021: Global Carbon and other Biogeochemical Cycles and Feedbacks. In *Climate Change 2021: The Physical Science Basis. Contribution of Working Group I to the Sixth Assessment Report of the Intergovernmental Panel on Climate Change* [Masson-Delmotte, V., P. Zhai, A. Pirani, S.L. Connors, C. Péan, S. Berger, N. Caud, Y. Chen, L. Goldfarb, M.I. Gomis, M. Huang, K. Leitzell, E. Lonnoy, J.B.R. Matthews, T.K. Maycock, T. Waterfield, O. Yelekçi, R. Yu, and B. Zhou (eds.)]. Cambridge University Press, Cambridge, United Kingdom and New York, NY, USA, pp. 673–816, doi:[10.1017/9781009157896.007](https://doi.org/10.1017/9781009157896.007).
- Chen, Z., Griffis, T. J., Millet, D. B., Wood, J. D., Lee, X., Baker, J. M., Xiao, K., Turner, P. A., Chen, M., Zobitz, J., & Wells, K. C. : Partitioning N<sub>2</sub>O emissions within the U.S. Corn Belt using an inverse modeling approach, *Global Biogeochemical Cycles*, 30(8), 1192–1205, <https://doi.org/10.1002/2015GB005313>, 2016.
- 585 Cheng, Y., Huang, M., Chen, M., Guan, K., Bernacchi, C., Peng, B., and Tan, Z.: Parameterizing perennial bioenergy crops in Version 5 of the Community Land Model based on site-level observations in the Central Midwestern United States, *Journal of Advances in Modelling Earth Systems*, 12, e2019MS001719. <https://doi.org/10.1029/2019MS001719>, 2020.
- Chiaravalloti, I. Observed ammonia fluxes during maize production in mesocosms with basalt amendments. *ESS Open Archive*, February 27, 2023, DOI: 10.22541/essoar.167751584.47065180/v1.
- 590 Crippa, M., Guizzardi, D., Muntean, M., Schaaf, E., Dentener, F., Van Aardenne, J. A., Monni, S., Doering, U., Olivier, J. G. J., Pagliari, V., and Janssens-Maenhout, G.: Gridded emissions of air pollutants for the period 1970–2012 within EDGAR v4.3.2, 10, 1987–2013, <https://doi.org/10.5194/essd-10-1987-2018>, 2018.
- Danabasoglu, G., Lamarque, J.-F., Bacmeister, J., Bailey, D. A., DuVivier, A. K., Edwards, J., et al.: The Community Earth System Model Version 2 (CESM2). *Journal of Advances in Modeling Earth Systems*, 12, e2019MS001916. <https://doi.org/10.1029/2019MS001916>, 2020.
- 595 Davidson, E. A. and Trumbore, S. E.: Gas diffusivity and production of CO<sub>2</sub> in deep soils of the eastern Amazon, *Tellus B*, 47, 550–565, <https://doi.org/10.1034/j.1600-0889.47.issue5.3.x>, 1995
- Davidson, E.A. and Verchot, L.V.: Testing the hole-in-the-pipe model of nitric and nitrous oxide emissions from soils using the TRAGNET data base, *Global Biogeochem. Cycles*, 14, 1035-1043, 2000.
- 600 Davidson, E. A. and Kanter, D.: Inventories and scenarios of nitrous oxide emissions, *Environ. Res. Lett.* 9, 105012, 2014.
- Del Grosso, S. J., Parton, W. J., Mosier, A. R., Ojima, D. S., Kulmala, A. E., & Phongpan, S.: General model for N<sub>2</sub>O and N<sub>2</sub> gas emissions from soils due to denitrification, *Global Biogeochemical Cycles*, 14, 1045–1060, <https://doi.org/10.1029/1999GB001225>, 2000.

- 605 Del Grosso, S. J., Parton, W. J., Mosier, A. R., Walsh, M. K., Ojima, D. S., & Thornton, P. E.: DAYCENT national-scale simulations of nitrous oxide emissions from cropped soils in the United States. *Journal of Environmental Quality*, 35, 1451–1460. <https://doi.org/10.2134/jeq2005.0160>, 2006.
- Drewniak, B., Song, J., Prell, J., Kotamarthi, V. R., and Jacob, R.: Modeling agriculture in the Community Land Model, *Geosci. Model Dev.*, 6, 495–515, <https://doi.org/10.5194/gmd-6-495-2013>, 2013.
- 610 European Environment Agency, EMEP/EEA air pollutant emission inventory guidebook 2013 – Technical guidance to prepare national emission inventories, Publications Office, <https://data.europa.eu/doi/10.2800/92722>, 2013
- Food and Agriculture organization (FAO) of the United Nations, Harmonized World Soil Database (version 1.2). Food Agriculture Organization, Rome, Italy and IIASA, Laxenburg, Austria, 2012.  
(<http://webarchive.iiasa.ac.at/Research/LUC/External-World-soil-database/HTML/>)
- 615 Firestone, M.K. and Davidson, E.A.: Microbiological Basis of NO and N<sub>2</sub>O Production and Consumption in Soils. In: Andreae, M.O. and Schimel, D.S., Eds., *Exchange of Trace Gases between Terrestrial Ecosystems and the Atmosphere*, John Willey and Sons, New York, 7-21, 1989.
- Fung, K. M., Val Martin, M., and Tai, A. P. K.: Modeling the interinfluence of fertilizer-induced NH<sub>3</sub> emission, nitrogen deposition, and aerosol radiative effects using modified CESM2, *Biogeosciences*, 19, 1635–1655, <https://doi.org/10.5194/bg-19-1635-2022>, 2022.
- 620 Griffis, T. J., Lee, X., Baker, J. M., Russelle, M. P., Zhang, X., Venterea, R., & Millet, D. B.: Reconciling the differences between top-down and bottom-up estimates of nitrous oxide emissions for the U.S. Corn Belt. *Global Biogeochemical Cycles*, 27(3), 746–754, <https://doi.org/10.1002/gbc.20066>, 2013.
- Goll, D.S., Ciais, P., Amann, T. *et al.* Potential CO<sub>2</sub> removal from enhanced weathering by ecosystem responses to powdered rock. *Nat. Geosci.* 14, 545–549 (2021). <https://doi.org/10.1038/s41561-021-00798-x>
- 625 Hoesly, R. M., Smith, S. J., Feng, L., Klimont, Z., Janssens-Maenhout, G., Pitkanen, T., Seibert, J. J., Vu, L., Andres, R. J., Bolt, R. M., Bond, T. C., Dawidowski, L., Kholod, N., Kurokawa, J., Li, M., Liu, L., Lu, Z., Moura, M. C. P., O'Rourke, P. R., and Zhang, Q.: Historical (1750–2014) anthropogenic emissions of reactive gases and aerosols from the Community Emissions Data System (CEDS), 11, 369–408, <https://doi.org/10.5194/gmd-11-825-369-2018>, 2018.
- 630 Hudman, R. C., Moore, N. E., Mebust, A. K., Martin, R. V., Russell, A. R., Valin, L. C., and Cohen, R. C.: Steps towards a mechanistic model of global soil nitric oxide emissions: implementation and space based-constraints, *Atmos. Chem. Phys.*, 12, 7779–7795, <https://doi.org/10.5194/acp-12-7779-2012>, 2012.
- Hurt, G. C., Chini, L. P., Frolking, S., Betts, R. A., Feddes, J., Fischer, G., Fisk, J. P., Hibbard, K., Houghton, R. A., Janetos, A., Jones, C. D., Kindermann, G., Kinoshita, T., Klein Goldewijk, K., Riahi, K., Shevliakova, E., Smith, S., Stehfest, E.,

- Thomson, A., Thornton, P., van Vuuren, D. P., and Wang, Y. P.: Harmonization of land-use scenarios for the period 1500–  
635 2100: 600 years of global gridded annual land-use transitions, wood harvest, and resulting secondary lands, *Clim. Change*,  
109, 117–161, <https://doi.org/10.1007/s10584-011-0153-2>, 2011.
- Inatomi M, Hajima T, Ito A. : Fraction of nitrous oxide production in nitrification and its effect on total soil emission: A meta-  
analysis and global-scale sensitivity analysis using a process-based model. *PLoS ONE* 14(7): e0219159.  
<https://doi.org/10.1371/journal.pone.0219159>, 2019.
- 640 IPCC, 2021: *Climate Change 2021: The Physical Science Basis. Contribution of Working Group I to the Sixth Assessment  
Report of the Intergovernmental Panel on Climate Change*[Masson-Delmotte, V., P. Zhai, A. Pirani, S.L. Connors, C. Péan,  
S. Berger, N. Caud, Y. Chen, L. Goldfarb, M.I. Gomis, M. Huang, K. Leitzell, E. Lonnoy, J.B.R. Matthews, T.K. Maycock,  
T. Waterfield, O. Yelekçi, R. Yu, and B. Zhou (eds.)]. Cambridge University Press, Cambridge, United Kingdom and New  
York, NY, USA, In press, doi:10.1017/9781009157896.
- 645 Jacob, D. J., and S. C. Wofsy : Budgets of reactive nitrogen, hydrocarbons and ozone over the Amazon forest during the wet  
season, *J. Geophys. Res.*, 95(D10), 16,737– 16,754, 1990.
- Johansson, C., Rodhe, H. and Sanhuenza, E. : Emission of NO in a tropical savanna and a cloud forest during the dry season,  
*J. Geophys. Res.*, 93(D6), 7180–7192, 1988.
- Kantzas, E.P., Val Martin, M., Lomas, M.R. et al.: Substantial carbon drawdown potential from enhanced rock weathering in  
650 the United Kingdom, *Nat. Geosci.* 15, 382–389, <https://doi.org/10.1038/s41561-022-00925-2>, 2022.
- Kim, M.-S.; Min, H.-G.; Koo, N.; Kim, J.-G: Response to Ammonia Emission Flux to different pH Conditions under Biochar  
and Liquid Fertilizer Application, *Agriculture*, 11, 136. <https://doi.org/10.3390/agriculture11020136>, 2022.
- Kantola, I. B., Masters, M.D., Beerling, D. J., Long, S. P., and DeLucia, E .H.: Potential of global croplands and bioenergy  
crops for climate change mitigation through deployment for enhanced weathering. *Biol. Lett.* 13, 20160714,  
655 <https://doi.org/10.1098/rsbl.2016.0714>, 2017.
- Koven, C. D., Riley, W. J., Subin, Z. M., Tang, J. Y., Torn, M. S., Collins, W. D., Bonan, G. B., Lawrence, D. M., and  
Swenson, S. C.: The effect of vertically resolved soil biogeochemistry and alternate soil C and N models on C dynamics of  
CLM4, *Biogeosciences*, 10, 7109–7131, <https://doi.org/10.5194/bg-10-7109-2013>, 2013.
- Lawrence, D., Fisher, R., Koven, C., Swenson, S., and Vertenstein, M.: Technical Description of version 5.0 of the Community  
660 Land Model (CLM), [http://www.cesm.ucar.edu/models/cesm2/land/CLM50\\_Tech\\_Note.pdf](http://www.cesm.ucar.edu/models/cesm2/land/CLM50_Tech_Note.pdf), last access: January 12, 2023.
- Lawrence, D. M., Fisher, R. A., Koven, C. D., Oleson, K. W., Swenson, S. C., Bonan, G., Collier, N., Ghimire, B.,  
Kampanhout, L., Kennedy, D., Kluzek, E., Lawrence, P. J., Li, F., Li, H., Lombardozzi, D., Riley, W. J., Sacks, W. J., Shi,  
M., Vertenstein, M., Wieder, W. R., Xu, C., Ali, A. A., Badger, A.M., Bisht, G., Broeke, M., Brunke, M. A., Burns, S. P.,

- Buzan, J., Clark, M., Craig, A., Dahlin, K., Drewniak, B., Fisher, J. B., Flanner, M., Fox, A. M., Gentine, P., Hoffman, F.,  
665 Keppel-Aleks, G., Knox, R., Kumar, S., Lenaerts, J., Leung, L. R., Lipscomb, W. H., Lu, Y., Pandey, A., Pelletier, J. D., Perket,  
J., Randerson, J. T., Ricciuto, D. M., Sanderson, B. M., Slater, A., Subin, Z. M., Tang, J., Thomas, R. Q., Val Martin, M., and  
Zeng, X.: The Community Land Model Version 5: Description of New Features, Benchmarking, and Impact of Forcing  
Uncertainty, *J. Adv. Model. Earth Syst.*, 11, 4245–4287, <https://doi.org/10.1029/2018MS001583>, 2019.
- Lawrence, P. J. and Chase, T. N.: Representing a new MODIS consistent land surface in the Community Land Model (CLM  
670 3.0), *J. Geophys. Res.*, 112, G01023, <https://doi.org/10.1029/2006JG000168>, 2007.
- Levis, S., Badger, A., Drewniak, B., Nevison, C., and Ren, X.: CLM crop yields and water requirements: avoided impacts by  
choosing RCP 4.5 over 8.5, *Clim. Change*, 146, 501–515, <https://doi.org/10.1007/s10584-016-1654-9>, 2018.
- Li, C., Narayanan, V., & Harriss, R. C.: Model estimates of nitrous oxide emissions from agricultural lands in the United  
States. *Global Biogeochemical Cycles*, 10(2), 297–306. <https://doi.org/10.1029/96GB00470>, 1996.
- 675 Li, C., Aber, J., Stange, F., Butterbach-Bahl, K. and Papen, H.: A process-oriented model of N<sub>2</sub>O and NO emissions from  
forest soils: 1. Model development. *J. Geophys. Res.* 105(D4):4369-4384, 2000.
- Li, C., Salas, W., Zhang, R., Krauter, C., Rotz, A., and Mitloehner, F.: Manure-DNDC: a biogeochemical process model for  
quantifying greenhouse gas and ammonia emissions from livestock manure systems, *Nutr. Cycl. Agroecosyst.*, 93, 163–200,  
<https://doi.org/10.1007/s10705-012-9507-z>, 2012.
- 680 Lin, H., Jacob, D. J., Lundgren, E. W., Sulprizio, M. P., Keller, C. A., Fritz, T. M., Eastham, S. D., Emmons, L. K., Campbell,  
P. C., Baker, B., Saylor, R. D., and Montuoro, R.: Harmonized Emissions Component (HEMCO) 3.0 as a versatile emissions  
component for atmospheric models: application in the GEOS-Chem, NASA GEOS, WRF-GC, CESM2, NOAA GEFS-  
Aerosol, and NOAA UFS models, *Geosci. Model Dev.*, 14, 5487–5506, <https://doi.org/10.5194/gmd-14-5487-2021>, 2021.
- Liu, B., Markved, P. T., Frostegård, ..., & Bakken, L. R.: Denitrification gene pools, transcription and kinetics of NO, N<sub>2</sub>O and  
685 N<sub>2</sub> production as affected by soil pH. *FEMS Microbiology Ecology*, 72, 407–417, <https://doi.org/10.1111/j.1574-6941.2010.00856.x>, 2010.
- Lombardozzi, D. L., Lu, Y., Lawrence, P. J., Lawrence, D. M., Swenson, S., Oleson, K. W., Wieder, W. R., and Ainsworth,  
E. A.: Simulating Agriculture in the Community Land Model Version 5, *J. Geophys. Res.-Biogeo.*, 125, e2019JG005529,  
<https://doi.org/10.1029/2019JG005529>, 2020
- 690 Lu, C., Yu, Z., Zhang, J., Cao, P., Tian, H., & Nevison, C.: Century-long changes and drivers of soil nitrous oxide (N<sub>2</sub>O)  
emissions across the contiguous United States. *Global Change Biology*, 28, 2505–2524, <https://doi.org/10.1111/gcb.16061>,  
2022.

- Martin, R. E., M. C. Scholes, A. R. Mosier, D. S. Ojima, E. A. Holland, and W. J. Parton: Controls on annual emissions of nitric oxide from soils of the Colorado shortgrass steppe, *Global Biogeochem. Cycles*, 12(1), 81–91, 1998.
- 695 Miller, S. M., Kort, E. A., Hirsch, A. I., Dlugokencky, E. J., Andrews, A. E., Xu, X., Tian, H., Nehrkorn, T., Eluszkiewicz, J., Michalak, A. M. and Wofsy, S. C.: Regional sources of nitrous oxide over the United States: Seasonal variation and spatial distribution, *Journal of Geophysical Research Atmospheres*, 117(6), D06310. <https://doi.org/10.1029/2011J D016951>, 2012.
- Mkhabela, M.S., Gordon, R., Burton, D. et al.: Effect of lime, dicyandiamide and soil water content on ammonia and nitrous oxide emissions following application of liquid hog manure to a marshland soil. *Plant Soil*, 284, 351–361.
- 700 <https://doi.org/10.1007/s11104-006-0056-6>, 2006.
- National Research Council, *Climate Intervention: Carbon Dioxide Removal and Reliable Sequestration*. Washington, DC: The National Academies Press. <https://doi.org/10.17226/18805>, 2015.
- Nevison, C., Andrews, A., Thoning, K., Dlugokencky, E., Sweeney, C., Miller, S., Saikawa, E., Benmergui, J., Fischer, M., Mountain, M., & Nehrkorn, T. : Nitrous oxide emissions estimated with the carbontracker-Lagrange North American regional inversion framework, *Global Biogeochemical Cycles*, 32(3), 463–485. <https://doi.org/10.1002/2017G B005759>, 2018.
- 705 Nevison, C., IPCC Good Practice Guidance and Uncertainty Management in National Greenhouse Gas Inventories, Indirect N<sub>2</sub>O emissions from nitrogen used in agriculture, [https://www.ipcc-nggip.iges.or.jp/public/gp/english/4\\_Agriculture.pdf](https://www.ipcc-nggip.iges.or.jp/public/gp/english/4_Agriculture.pdf), 2021, Last accessed February 9, 2023.
- Nevison, C., Goodale, C., Hess, P., Wieder, W. R., Vira, J. and Groffman, P.M.: Nitrification and Denitrification in the Community Land Model Compared with Observations at Hubbard Brook Forest, *Ecological Applications* e2530. <https://doi.org/10.1002/eap.2530>, 2022a.
- 710 Nevison, C., Hess, P., Goodale, C., Zhu, Q. and Vira, J.: Nitrification, Denitrification, and Competition for Soil N: Evaluation of Two Earth System Models against Observations, *Ecological Applications* e252, <https://doi.org/10.1002/eap.2528>, 2022b.
- Parton, W. J., Mosier, A. R., Ojima, D. S., Valentine, D. W., Schimel, D. S., Weier, K., & Kulmala, A. E.: Generalized model for N<sub>2</sub> and N<sub>2</sub>O production from nitrification and denitrification. *Global Biogeochemical Cycles*, 10, 401–412. <https://doi.org/10.1029/96GB0 1455>, 1996.
- 715 Parton, W. J., Holland, E. A., Del Grosso, S. J., Hartman, M. D., Martin, R. E., Mosier, A. R., Ojima, D. S., & Schimel, D. S.: Generalized model for NO<sub>x</sub> and N<sub>2</sub>O emissions from soils. *Journal of Geophysical Research: Atmospheres*, 106, 17403–17419. <https://doi.org/10.1029/2001J D900101>, 2001.
- 720 Paulot, F., Jacob, D. J., Pinder, R. W., Bash, J. O., Travis, K., and Henze, D. K.: Ammonia emissions in the United States, European Union, and China derived by highresolution inversion of ammonium wet deposition data: Interpretation with a new

- agricultural emissions inventory (MASAGE\_NH<sub>3</sub>), *J. Geophys. Res.-Atmos.*, 119, 4343–4364, <https://doi.org/10.1002/2013JD021130>, 2014.
- Portmann, F. T., Siebert, S., and Döll, P.: MIRCA2000-Global monthly irrigated and rainfed crop areas around the year 2000: 725 A new high-resolution data set for agricultural and hydrological modelling: MONTHLY IRRIGATED AND RAINFED CROP AREAS, *Global Biogeochem. Cy.*, 24, GB1011, <https://doi.org/10.1029/2008GB003435>, 2010.
- Prather, M. J. et al.: Measuring and modelling the lifetime of nitrous oxide including its variability, *J. Geophys. Res. D* 120, 5693–5705, 2015.
- Reay, D. S. et al.: Global agriculture and nitrous oxide emissions, *Nat. Clim. Change* 2, 410–416, 2012.
- 730 Riahi, K., Bertram, C., Huppmann, D. *et al.* Cost and attainability of meeting stringent climate targets without overshoot. *Nat. Clim. Chang.* 11, 1063–1069 (2021). <https://doi.org/10.1038/s41558-021-01215-2>
- Royal Society and Royal Academy of Engineering, Greenhouse gas removal ISBN: 978-1-78252-349-9, <https://royalsociety.org/topics-policy/projects/greenhouse-gas-removal/> (Last accessed 31 January, 2023), 2018.
- Rochester, I. J.: Estimating nitrous oxide emissions from flood-irrigated alkaline grey clays, *Soil Research*, 41, 197–206. 735 <https://doi.org/10.1071/sr02068>, 2003.
- Saikawa, E., Prinn, R. G., Dlugokencky, E., Ishijima, K., Dutton, G. S., Hall, B. D., Langenfelds, R., Tohjima, Y., Machida, T., Manizza, M., Rigby, M., O'Doherty, S., Patra, P. K., Harth, C. M., Weiss, R. F., Krummel, P. B., van der Schoot, M., Fraser, P. J., Steele, L. P., Aoki, S., Nakazawa, T., and Elkins, J. W.: Global and regional emissions estimates for N<sub>2</sub>O, *Atmos. Chem. Phys.*, 14, 4617–4641, <https://doi.org/10.5194/acp-14-4617-2014>, 2014.
- 740 Sha Z., Qianqian Li, Tiantian Lv, Tom Misselbrook, Xuejun Liu: Response of ammonia volatilization to biochar addition: A meta-analysis, *Science of The Total Environment*, 655, 1387-1396, ISSN 0048-9697, [https://doi.org/10.1016/j.scitotenv.2018.11.316\\_2019](https://doi.org/10.1016/j.scitotenv.2018.11.316_2019).
- Shcherbak I., Millar, N., and Robertson, G.P.: Global metaanalysis of the nonlinear response of soil nitrous oxide (N<sub>2</sub>O) 745 emissions to fertilizer nitrogen, *PNAS* 111, 9199-9204, 2014.
- Smith, S. M., Geden, O., Nemet, G., Gidden, M., Lamb, W. F., Powis, C., Bellamy, R., Callaghan, M., Cowie, A., Cox, E., Fuss, S., Gasser, T., Grassi, G., Greene, J., Lück, S., Mohan, A., Müller-Hansen, F., Peters, G., Pratama, Y., Repke, T., Riahi, K., Schenuit, F., Steinhauser, J., Strefler, J., Valenzuela, J. M., and Minx, J. C. (2023). The State of Carbon Dioxide Removal - 750 1st Edition. The State of Carbon Dioxide Removal. doi:10.17605/OSF.IO/W3B4Z

- Stehfest, E. and Bouwman, L.: N<sub>2</sub>O and NO Emission from Agricultural Fields and Soils under Natural Vegetation: Summarizing Available Measurement Data and Modeling of Global Annual Emissions. *Nutrient Cycling in Agroecosystems*, 74, 207-228. 597 <http://dx.doi.org/10.1007/s10705-006-9000-7>, 2006.
- 755 Syakila, A., & Kroeze, C.: The global nitrous oxide budget revisited. *Greenhouse Gas Measurement and Management*, 1(1), 17–26., <https://doi.org/10.3763/ghgmm.2010.0007>, 2011.
- Sutton, M. A., Reis, S., Riddick, S. N., Dragosits, U., Nemitz, E., Theobald, M. R., Tang, Y. S., Braban, C. F., Vieno, M., Dore, A. J., Mitchell, R. F., Wanless, S., Daunt, F., Fowler, D., Blackall, T. D., Milford, C., Flechard, C. R., Loubet, B., Massad, R., Cellier, P., Personne, E., Coheur, P. F., Clarisse, L., Van Damme, M., Ngadi, Y., Clerbaux, C., Skjøth, C. A., Geels, C., Hertel, O., Wichink Kruit, R. J., Pinder, R. W., Bash, J. O., Walker, J. T., Simpson, D., Horváth, L., Misselbrook, 760 T. H., Bleeker, A., Dentener, F., and de Vries, W.: Towards a climate-dependent paradigm of ammonia emission and deposition, *Philos. T. Roy. Soc. B*, 368, 20130166, <https://doi.org/10.1098/rstb.2013.0166>, 2013.
- Tian, H., Yang, J., Lu, C., Xu, R., Canadell, J. G., Jackson, R. B., Arneeth, A., Chang, J., Chen, G., Ciais, P., Gerber, S., Ito, A., Huang, Y., Joos, F., Lienert, S., Messina, P., Olin, S., Pan, S., Peng, C., Zhu, Q.: The global N<sub>2</sub>O model intercomparison project, *Bulletin of the American Meteorological Society*, 99(6), 1231–1251. <https://doi.org/10.1175/BAMS-D-17-0212.1>, 765 2018.
- Tian, H., Yang, J., Xu, R., Lu, C., Canadell, J. G., Davidson, E. A., Jackson, R. B., Arneeth, A., Chang, J., Ciais, P., Gerber, S., Ito, A., Joos, F., Lienert, S., Messina, P., Olin, S., Pan, S., Peng, C., Saikawa, E., Zhang, B.: Global soil nitrous oxide emissions since the preindustrial era estimated by an ensemble of terrestrial biosphere models: Magnitude, attribution, and uncertainty. *Global Change Biology*, 25(2), 640–659. <https://doi.org/10.1111/gcb.14514>, 2019.
- 770 U.K. Department for Environment, Food and Rural Affairs (DEFRA), Clean Air Strategy 2019, <https://www.gov.uk/government/publications/clean-air-strategy-2019>, last access: 25 January 2023.
- U.S. Environmental Protection Agency (EPA), The Particle Pollution Report: Current Understanding of Air Quality and Emissions through 2003; EPA 454-R-04-002; U.S. Government Printing Office: Washington, DC, 2004.
- U.S. Environmental Protection Agency (EPA): Inventory of U.S. Greenhouse Gas Emissions and Sinks: 1990-2020. U.S. 775 Environmental Protection Agency, EPA 430-R-22-003, <https://www.epa.gov/ghgemissions/draft-inventory-us-greenhouse-gas-emissions-and-sinks-1990-2020>, 2022.
- Van Damme, M., Clarisse, L., Franco, B., Sutton, M.A., Willem Erisman, J., Wichink Kruit, R., van Zanten, M., Whitburn, S., Hadji-Lazaro, J., Hurtmans, D., Clerbaux, C., Coheur, P.-F: Global, regional, and national trends of atmospheric ammonia derived from a decadal (2008-2018) satellite record, *Environ. Res. Lett.* 16 <https://doi.org/10.1088/1748-9326/abd5e0>, 2021.
- 780 Vieno, M., Heal, M. R., Williams, M. L., Carnell, E. J., Nemitz, E., Stedman, J. R., and Reis, S.: The sensitivities of emissions reductions for the mitigation of UK PM<sub>2.5</sub>, *Atmos. Chem. Phys.*, 16, 265–276, <https://doi.org/10.5194/acp-16-265-2016>, 2016.

- Vira, J., Hess, P., Melkonian, J., and Wieder, W. R.: An improved mechanistic model for ammonia volatilization in Earth system models: Flow of Agricultural Nitrogen version 2 (FANv2), *Geosci. Model Dev.*, 13, 4459–4490, <https://doi.org/10.5194/gmd-13-4459-2020>, 2020.
- 785 Wagena, M. B., Bock, E. M., Sommerlot, A. R., Fuka, D. R., & Easton, Z. M.: Development of a nitrous oxide routine for the SWAT model to assess greenhouse gas emissions from agroecosystems. *Environmental Modelling and Software*, 89, 131–143. <https://doi.org/10.1016/j.envsoft.2016.11.013>, 2017.
- Wang, Q., Feng Zhou, Ziyin Shang, Philippe Ciais, Wilfried Winiwarter, Robert B Jackson, Francesco N Tubiello, Greet Janssens-Maenhout, Hanqin Tian, Xiaoqing Cui, Josep G Canadell, Shilong Piao, Shu Tao: Data-driven estimates of global nitrous oxide emissions from croplands, *National Science Review*, 7, 2, 441–452, <https://doi.org/10.1093/nsr/nwz087>, 2020.
- 790 Wang, Y., Guo, J., Vogt, R.D., Mulder, J., Wang, J., and Zhang, X: Soil pH as the chief modifier for regional nitrous oxide emissions: New evidence and implications for global estimates and mitigation, *Global Change Biology* 24, 617–626, 2018.
- Wieder, W.R., J. Boehnert, G.B. Bonan, and M. Langseth: RegridDED Harmonized World Soil Database v1.2. Data set. Available on-line [<http://daac.ornl.gov>] from Oak Ridge National Laboratory Distributed Active Archive Center, Oak Ridge, Tennessee, USA, <http://dx.doi.org/10.3334/ORNLDAAAC/1247>, 2014.
- 795 Wyer, K. E., Kelleghan, D. B., Blanes-Vidal, V., Schaubberger, G., Curran, T. P.: Ammonia emissions from agriculture and their contribution to fine particulate matter: A review of implications for human health, *Journal of Environmental Management*, Volume 323, 116285, ISSN 0301-4797, <https://doi.org/10.1016/j.jenvman.2022.116285>, 2022.
- Xia, Y., Mitchell, K., Ek, M., Sheffield, J., Cosgrove, B., Wood, E., et al.: Continental-scale water and energy flux analysis and validation for the North American Land Data Assimilation System project phase 2 (NLDAS-2): 1. Intercomparison and application of model products. *Journal of Geophysical Research*, 117, D03109, <https://doi.org/10.1029/2011JD016048>, 2012.
- 800 Yan, X., Ohara, T., and Akimoto, H.: Statistical modelling of global soil NO<sub>x</sub> emissions, *Global Biogeochem. Cy.*, 19, GB3019, doi:10.1029/2004GB002276, 2005.
- Yienger, J. J. and Levy II, H.: Empirical model of global soil biogenic NO<sub>x</sub> emissions, *J. Geophys. Res.*, 100, 11447–11464, 805 1995.
- Yoneyama, T., Hashimoto, A. and Totsuka, T.: Absorption of atmospheric NO<sub>2</sub> by plants and soils, *Soil Science and Plant Nutrition*, 26:1, 1-7, DOI: 10.1080/00380768.1980.10433207, 1980.
- Zeri, M., Anderson-Teixeira, K., Hickman, G., Masters, M., DeLucia, E., & Bernacchi, C. J.: Carbon exchange by establishing biofuel crops in Central Illinois. *Agriculture, Ecosystems and Environment*, 144(1), 319–329. 810 <https://doi.org/10.1016/j.agee.2011.09.006>, 2011.



Zhao, Y., Zhang, L., Tai, A. P. K., Chen, Y., and Pan, Y.: Responses of surface ozone air quality to anthropogenic nitrogen deposition in the Northern Hemisphere, 17, 9781–9796, <https://doi.org/10.5194/acp-17-9781-2017>, 2017.

815